Published in final edited form as:
Nanomedicine (Lond). 2009 October ; 4(7): 813–845. doi:10.2217/nnm.09.59.

Plasmonic nanoparticle-generated photothermal bubbles and their biomedical applications

Dmitri Lapotko
AV Lykov Heat & Mass Transfer Institute, 15 P Brovka St., Minsk 220072, Belarus and Department of Physics & Astronomy, Rice University, 6100 Main Street, Houston, TX 77005, USA, Tel.: +1 713 348 3708; Fax: +1 713 348 3708; dl5@rice.edu

Abstract

This article is focused on the optical generation and detection of photothermal vapor bubbles around plasmonic nanoparticles. We report physical properties of such plasmonic nanobubbles and their biomedical applications as cellular probes. Our experimental studies of gold nanoparticle-generated photothermal bubbles demonstrated the selectivity of photothermal bubble generation, amplification of optical scattering and thermal insulation effect, all realized at the nanoscale. The generation and imaging of photothermal bubbles in living cells (leukemia and carcinoma culture and primary cancerous cells), and tissues (atherosclerotic plaque and solid tumor in animal) demonstrated a noninvasive highly sensitive imaging of target cells by small photothermal bubbles and a selective mechanical, nonthermal damage to the individual target cells by bigger photothermal bubbles due to a rapid disruption of cellular membranes. The analysis of the plasmonic nanobubbles suggests them as theranostic probes, which can be tuned and optically guided at cell level from diagnosis to delivery and therapy during one fast process.

Keywords

cell; imaging; laser; plasmonic nanoparticle; photothermal; theranostics; vapor bubble

---

Biomedical applications of plasmonic nanoparticles (NPs) have demonstrated their biocompatibility [1,2], excellent optical scattering [3–7] and photothermal (PT) [8–12] properties and high photo- and thermal stability in comparison to any molecular optical absorbers. The combination of PT-sensing techniques [13] with plasmonic properties of the NPs has shown very promising results with a detection limit of several nanometers [14]. However, the sensitivity of PT sensing requires an increase in the laser-induced temperature, which may cause thermal damage to cells and tissues. Laser-induced PT phenomena include the initial thermalization of NPs that, in turn, rapidly causes several environmental thermal processes: the heating of the surrounding media [15–17] (due to thermal diffusion), its vaporization (if the temperature exceeds the vaporization threshold) and the generation of acoustic and shock waves [18]. Pulses that are too long (or continuous optical activation) cause a large spatial spread of the thermal field (many orders of magnitude larger than NP size) due to the thermal diffusion. This limits the selectivity and safety of NP-based PT diagnostics and therapy. Ultra-short laser pulses concentrate the thermal field within the NP but generate pressure (and shock) waves that also spread over a large volume and may cause uncontrollable damage [19]. The sensitivity, safety and specificity of NP methods are limited at cell and molecular levels by the strong scattering background of a highly heterogeneous bio-environment and also by the incidental (nonspecific) accumulation of NPs in normal cells and tissues. Therefore, despite the apparent advantages of nanomaterials, their biomedical application does not yet bring a significant gain on the established methods.

The laser-induced evaporation and cavitation around NPs still remain the most under-recognized phenomena among the PT effects of the optical excitation of plasmon NPs. The optical generation and detection of tissue-generated vapor bubbles was studied at macro- and micro-scales for different biomedical applications [18,20–23]. However, studies of the bubble generation around laser-heated NPs [12,24,25] and at the nanoscale [26] are rather limited. The properties of NP-generated nanobubbles are quite different from their macroanalogs. For example, for macrobubbles the generation threshold laser fluence increases with an increase of the size of the optical absorber (bubble source) [27], while for the NP-generated bubbles this rule is the opposite: the bigger the size of plasmonic NPs the lower the laser fluence threshold for the bubble generation [28,29]. The bubbles are also used as ultrasound-induced therapeutics and for imaging extracellular agents [30–32]. However, acoustic methods have a low selectivity and poor temporal and spatial resolution of the bubble generation (well above a cell damage level), which preclude intracellular applications. High-intensity focused ultrasound techniques were developed for therapy but besides a low selectivity they require a prolonged treatment time, are associated with significant adverse effects and need additional guidance during the procedure. In addition, artificially engineered microparticles with a gas inside are employed with the ultrasound for hyperthermia and imaging. Those exogenous bubbles are too big for the intracellular targeting in comparison with gold NPs and do not allow the generation of local thermomechanical effects. We may conclude that the optical and acoustic activation of diagnostic and therapeutic processes lacks selectivity and therefore still has limited efficacy and safety.

There are several general issues that influence the development of diagnostic and therapeutic methods and agents:

- Separate diagnostics, therapy and verification (guidance) of the therapy extends the time of treatment and increases the load on a target or organism. The possibility of using one method (theranostics), device and agent for all of these steps would ultimately make the treatment shorter, safer and more efficient;
- Disease (especially in the early stage) can be represented by a few specific cells that are often mixed with normal tissue, while the therapeutic impact affects not only pathological cells but also normal ones. This lack of selectivity also decreases the efficacy and safety of the treatment;
- The toxicity of some probes that have yielded a high sensitivity and efficacy at the research stage often prevents their transfer to the clinic.

We hypothesized that a combination of the properties of plasmonic NPs with those of the PT vapor bubbles may be a key solution to the above problems through the development of a tunable nanoscale imaging, diagnostic and therapeutic agent/process (Figure 1). NP-generated vapor bubbles may concentrate the laser-induced thermal field and mechanical (pressure) impact around NPs. Maximal size and lifetime of the bubble can be tuned in the range of 50–1000 nm and 5–500 ns, respectively, with the parameters of laser pulse. In addition, bubbles possess excellent optical scattering properties [33–35], which may help with their detection at the nanoscale and improve the NP-based optical sensing and imaging through the amplification of the scattered light by orders of magnitude relative to that of NPs. Despite the basically disruptive nature of bubbles it has been experimentally determined that optically or acoustically generated bubbles of small size may not damage cells [12,36–38]. Target-specific generation of the bubbles can be realized through the delivery of small functionalized NPs (which can enter the cell while big NPs cannot) and intracellular formation of their clusters. The NP cluster, selectively formed around target molecules, will act as the bubble source (Figure 1), while no bubble would be generated around single nonspecifically coupled NPs at the specific level of a laser fluence. Thus we will selectively generate the bubble as an optical probe (acting through optical scattering) and/or a therapeutic agent (acting through a mechanical impact) in the right

place (a target-linked NP cluster) and at the right time (a single short optical pulse). To distinguish the optical and thermal origin of such bubbles we define them as the PT bubbles (PTBs). It also should be emphasized that the generation and detection of PTBs do not require chemical agents, other than relatively safe gold NPs. The safe and universal nature of the gold NP-generated PTBs may shorten the transfer of PTB-based technologies from the research stage to the clinic.

This work is a focused review of our previous experimental studies of the mechanisms of PTB generation and detection around gold NPs, of PTB interactions with living cells, and biomedical properties of NP-generated PTBs. The main purpose of this review was to formulate a new concept of PTB theranostics at a cellular level. Theranostics (combining diagnosis and therapy in one process) is an emerging approach in medicine [39,40]. A distinct goal of such an approach is to selectively target diseased tissues or cells to increase the diagnostic and therapeutic accuracy. Theranostic methods have employed various NPs, although only as carriers of diagnostic agents and drugs [41–43]. However, our previous works demonstrate that plasmonic NPs may act as active theranostics agents even without any chemical loads by use of the PTB mechanism. The optical monitoring of disruptive PTBs can also evaluate their therapeutic action. Thus, NP-generated PTBs may combine diagnostics, therapy and therapy guidance into one fast process. Theranostics has not been previously considered in studies of PT and scattering effects of plasmonic NPs, and for this reason we did not review all published biomedical applications of NP-generated PT effects but have focused on the experimentally established properties of the NP-generated PTBs. The mechanisms of NP-PTB optical generation and detection were described in the next section and the biomedical properties of intracellular and tissue-generated NP-PTBs are described in another section.

Plasmonic NP-generated PTBs

Generation of PTBs

Evaporation of the medium around a NP involves several processes. Laser pulse-induced thermalization of the NP occurs in approximately 1 ps [15,44–46], and the temperature of the NP may reach, or even exceed, its melting point (1337 K for gold). Next, thermal diffusion from the NP to the adjusting medium delivers thermal energy required for its evaporation. Formation of a thin vapor layer around the NP creates the PTB nucleus. The PTB develops from the nucleus providing that sufficient initial potential energy was deposited so as to overcome opposing forces of the surface tension and viscosity. After the bubble emerges, it undergoes the expansion to maximal diameter and collapse. Bubble lifetime may be considered as linearly proportional to its maximal diameter [20,22,47–50]. The minimal fluence of single laser pulse that provides bubble generation is defined as the PTB generation threshold fluence. While the mechanism of the bubble evolution is well studied, the transition from the NP optical excitation to the PTB is less understood. We have estimated the spatial and temporal conditions of the deposition of thermal energy into the nanovolume around the NP. If the localization of PT impact is required, there should be no pressure and shock wave, and also the thermal-diffusion losses should be minimized. The conditions for the generation of pressure waves and the thermal diffusion can be expressed through the diameter D_{np} of the NP as the acoustic:

$$\tau_a = \frac{D_{np}}{C_g}$$

and thermal:

$$\tau_t = \frac{D_{np}^2}{24a}$$

relaxation times, respectively, where c_g is the speed of sound in the NP and a is the thermal conductivity of surrounding media (Figure 2).

When the optical pulse duration $\tau_l > \tau_a$ no pressure or shock wave would emerge. When $\tau_l < \tau_t$ the losses due to thermal diffusion are negligible and all released heat is concentrated in small volume around the heat source. Thus, we may classify the NP-related PT processes in terms of their scale and nature as microthermal mode, nanothermal mode, and nanothermal pressure wave mode (Figure 2). In many cases the NPs may aggregate into a cluster [51,52], which acts as a solid thermal source of a much bigger diameter than a single NP. An advantage of the cluster over the single NP of the same diameter is the much bigger surface of the NP–environment border in the case of the cluster. This significantly enhances heat transfer from the NP to the environment and thus stimulates formation of one joint bubble nucleus in the cluster. Such a nucleus may accumulate more energy than a single NP-formed nucleus and, therefore, NP clusters allow generation of the bubble at a lower fluence of pump laser pulse. The grey area in Figure 2 shows the optimal conditions of local heating of the media around the NP: minimal heat losses and no pressure waves. In this case the released energies are efficiently used for local heating and evaporation.

Optical detection of PTBs around gold NPs

Bubble generation was studied in water suspensions of NPs by exposing the sample to a single 0.5 ns laser pulse at a wavelength close to that of plasmon resonance for the NPs. We have exposed the sample with 30-nm gold nano-spheres (NSPs; water suspension at 10^{11}/ml) to single 0.5 ns laser pulses at gradually increasing fluence levels. All samples were studied in closed cuvettes, having diameter 9 mm and height 10 μm. Optical scattering images were obtained prior to pump pulse (Figure 3A & C) and at a specific time delay (9 ns) after the pump pulse (Figure 3B & D). Responses were obtained simultaneously with the pump pulse (Figure 4). Without the pump pulse, the scattering from single NPs was too weak to form detectable images of single NPs and did not exceed the scattering from the bulk media (background). The exposure to single pump laser pulses at a fluence starting from 0.5–0.6 J/cm^2 resulted in the appearance of bright diffraction-limited spots in the time-resolved images and symmetrical dip-shaped responses in the durations starting from 15 ns (Figure 4A).

These signals characterize optical scattering by the PTB: the image shows its location (the NP concentration was low enough so as to prevent any ensemble effects) and the response shows the bubble dynamics – expansion and collapse. These signals also deliver two quantitative measures of the PTB: the image pixel amplitude characterizes the current PTB diameter and the response duration characterizes the PTB lifetime (which, in turn, characterizes the maximal diameter of the PTB, see Table 1). Both parameters depend upon initial energy that was transferred into the PTB from the plasmonic NP and they generally directly express the two most important biomedical properties of the PTB: brightness (diagnostic property) and mechanical impact (therapeutic property). Additional details can be found in [29,53–56].

The effect of NP clustering

Clustering of 30-nm NSPs (prepared by adding acetone into water suspension of the NPs) significantly increased the scattering amplitudes compared with single NPs (Figure 3C & Table 1). The exposure of NP clusters to a pump laser pulse caused bright spots in scattering images (Figure 3D) that spatially coincided with NP clusters (in the optical scattering image). Pixel

amplitudes of the images and lifetimes of cluster-generated PTBs increased and the threshold fluence of PTB generation significantly decreased compared with those for single NPs (Table 1). The PTB generation thresholds were determined by measuring the probabilities of the PTB generation in image and response modes as a function of laser fluence. The threshold fluence corresponds to the probability value of 0.5.

The probability of PTB generation in image mode was found to be higher than that measured in response mode. Thus, the image mode yielded the PTB generation threshold as 0.088 J/cm^2 while the response mode yielded the PTB generation threshold as 0.3 J/cm^2 for the same sample (clusters of 30-nm NSPs). Therefore, the sensitivity of PTB detection in image mode is higher than in response mode. All PTBs were observed during the first pump pulse. In the case of single NPs, we observed no PTB generation during repeated exposures of the same area of sample. This could have been caused by continuous NP motion in the water or by their photodamage. In the case of optically detectible and stationary NP clusters, the PTBs were reproducible at the level of pump laser fluence close to the PTB generation threshold. However, at increased pump fluence the PTBs deteriorated within four–eight pulses applied with 1–3 s intervals. Based on the above results, we may conclude that the generation of PTBs around NPs has a threshold nature, that PTBs may be optically detected and that the clustering of the NPs significantly improves the conditions of PTB generation by decreasing its threshold fluence and increasing its lifetime (and hence the maximal size of the PTB). According to the images obtained, the PTBs generated at fluencies close to and above the threshold were of submicrometer size because they produced diffraction-limited images.

We used the response mode to study PTB lifetime (which also characterizes maximal PTB size) as a function of laser fluence and of NP aggregation state (Figure 5A). Both single NPs and their clusters generated PTBs starting from a specific threshold of laser fluence (Figure 5A & Table 1). This fluence level was almost one order of magnitude lower for the NP clusters relative to that for single NPs. This also means that clusters generate PTBs at much lower initial laser-induced temperatures. Lifetimes of the PTBs at threshold fluences were in the range of 15 to 25 ns and did not differ much between the clusters and single NPs. This means that different heat nanosources produce similar minimal bubbles at threshold conditions. The shortest detected lifetime of a PTB regardless of the NP type, size and state was approximately 15 ns. The difference between single NPs and their clusters became apparent with an increase of laser fluence. The slope of the lifetime–fluence graph was much higher for clusters than for single NPs and, furthermore, the clusters allowed generation of much bigger PTBs (with lifetimes of several hundred ns) at moderate levels of laser fluence (within 1 J/cm^2), while almost no PTBs were detected around single NPs at the same fluence level. Therefore, the clustering of NPs also improves selectivity of PTB generation: at a specific level of laser fluence PTBs emerge only around NP clusters and will not emerge around single NPs. We have found that PTB lifetime almost linearly increased with the increase of pump laser fluence (both for NPs and their clusters) and thus the maximal diameter of PTBs can be controlled though the level of laser pulse fluence (Figure 5A). Additional details can be found in [29,51,55–58].

Laser-induced thermal field around NPs & PTBs

Careful examination of the responses obtained for NP suspension at laser fluence levels below the PTB generation threshold has yielded a weak thermal signal (Figure 4C) that had a relatively sharp front (10–20 ns) and a long, gradual tail of micro-second length (shown in the insert of Figure 4C with full timescale). This signal indicates that the residual thermal field has emerged around the NP and describes the dynamics (heating and cooling) of the bulk temperature that was induced due to thermal diffusion from laser-heated NPs. As can be seen from Figure 4C, bulk temperature rise shifts the response amplitude from the baseline, thus indicating the difference in the temperatures before and after exposure to the pump laser pulse. Comparison

of these 'thermal' responses (Figure 4C) with the PTB responses (Figure 4A & B) has revealed a rather important feature of NP-generated PTBs: after PTB collapse, the response amplitude returned to its baseline level, which indicates that the residual bulk temperature did not differ from the initial one (prior to pump laser pulse). In other words, in the case of a PTB there was no residual heating of the bulk media, as has been found for nonbubble conditions (Figure 4C). In case of PTB generation, the initial laser-induced temperature around NP was higher than that induced with lower fluence (Figure 4C). Despite the increased initial heating of the NP, the PTB apparently consumes almost all of the thermal energy and prevents heating of the microenvironment. This effect partly corresponds to the results obtained with the other type of optically absorbing NPs [59]. We have observed no other processes that may utilize PTB energy during their generation: there was no oscillation of the bubbles and no signals that can be attributed to pressure waves generated by NPs. For a better understanding of this result we studied PTB generation in a homogeneously absorbing solution without plasmonic NPs. The obtained PTB response (Figure 4D) showed the two superimposed processes: a PTB and bulk thermal field. Homogeneously absorbing media is almost uniformly heated during absorption of laser pulse and this caused the combination of the PTB and thermal responses. In the case of NP suspension, the temperature field is highly nonuniform, with maximal temperature localized around the NPs. Explanation of the discovered 'no heating' phenomenon requires further study of the mechanism of NP-generated PTBs and is beyond the scope of this work. Nevertheless, this finding shows the principal difference between NP-generated nanobubbles and laser-induced macrobubbles. Additional details can be found in [28,60].

Influence of laser & NP parameters on the properties of PTBs

All results described above were obtained for a specific laser pulse duration, NP type, NP size and size of sample chamber. We have also explored the influence of the above parameters on PTB generation [55]. The laser pulse duration was increased to 10 ns, while the wavelength and beam geometry were identical to those of the 0.5 ns pulse. Samples included gold NSPs increased to 100 nm diameter, gold nanorods (NRs) 14 × 45 nm, clusters of silica–gold nanoshells (NSs) with outer diameters of 60 and 170 nm and with broad extinction spectra. All experiments were performed in response mode for a single laser pulse.

The increase of the laser pulse length by 20-fold caused a 13–24-fold increase in PTB-generation threshold fluence in all studied NPs and their clusters (Figure 6A). Decreased efficacy of PTB generation could result from increased thermal losses in the case of long pulse as shown in Figure 1. It may be also possible that PTBs scatter the incident long pulse, thus decreasing its actual fluence. As can be seen from Figure 6B, PTB lifetimes were almost equal at threshold fluences for short and long laser pulses and thus the increase of pulse length did not influence the maximal diameters of the PTBs. The reproducibility of the PTBs was also the same for short pulses – the PTBs were not reproducible for single NPs and exhibited rapid deterioration when generated around NP clusters.

Next, we compared different types of NPs and their clusters. The increase of the NP NSP diameter from 30 to 100 nm has decreased PTB generation threshold fluence by several times. Thus, the increase of NP size lowers the PTB generation threshold. For bubbles generated around microabsorbers this rule is the opposite: the bigger the absorber the higher the PTB generation threshold [27,61]. Minimal PTB generation thresholds were achieved with NP clusters regardless of the type of NP (NSPs and two different types of NS). We have found that the increase of cluster size (estimated with optical microscopy) has also lowered PTB generation threshold (Figure 6): gold 60 nm NS clusters of 500–700 nm (the biggest ones) have yielded the lowest PTB generation threshold fluence of 12 mJ/cm^2 (while for unclustered 60 nm gold NSs, the PTB generation threshold was 180 mJ/cm^2 [15-times higher] and for smaller clusters [100–300 nm] of 30 nm NSPs the PTB generation threshold was found to be 200 mJ/

cm^2, or approximately 17-times higher than that for the 60 nm NS clusters). NP clusters also exhibited good reproducibility of PTBs during repeated exposure of one cluster to several laser pulses that were applied with 1–5 s intervals, while for the single NPs the bubbles were not reproducible after their exposure to a single high-energy pump laser pulse. This effect may be caused by thermal destruction or shape modification of the single NPs. Theoretically, the same mechanisms should act also in the cluster of NPs. However, NP clusters have demonstrated the reproducibility of PTBs after up to 20 laser pulses. There are several potential explanations for this difference: the cluster may provide the condensation of melted NPs in the same place; the cluster may screen some NPs from being thermally destroyed so they survive laser pulses; and the much bigger radius of the vapor nucleus around the cluster creates a much lower surface tension around it, thus providing PTB generation at a significantly lower temperature and hence without severe damage to the NPs. Therefore, NP clusters may be considered as the best solution (relative to NPs and other optical absorbers) for minimizing PTB generation fluence and temperature thresholds.

We have measured the probability and threshold of PTB generation as functions of NP diameter and NP concentration. The influence of NP diameter was studied at minimal concentrations (2.6×10^8/ml) so as to ensure that PTBs are generated around a single NP. This concentration corresponds to the average distance between the NPs being 15.7 μm. A single laser pulse was used to obtain the probability of PTB generation at several specific levels of pulse fluences. After the dependence probability versus fluence was acquired, the threshold level of laser fluence that corresponds to a 0.5 probability of PTB generation was derived from the probability curve. This experiment was performed separately for each diameter of NP. We found that decreasing NP diameter from 250 nm to 30 nm (8.3-times) caused an increase in the PTB generation threshold, from 0.35 to 36.9 J/cm^2 (105-times) (Figure 7A). Such strong dependence is nanoscale-specific [27]. The obtained result also means that formally a much lower temperature (two orders of magnitude in this case) is required for the generation of PTBs around bigger NPs. In addition, we may assume from the shape of the obtained curve that the smaller the NP, the stronger the influence of its diameter on the PTB generation threshold. The influence of NP concentration (which determines the average distance between each NP) was measured for 30-nm NSPs (Figure 7B). The concentration of NPs in water varied from 2×10^{11}/ml to 2.6×10^8/ml, which corresponds to the average interparticle distance x varying from 1.7 to 15.7 μm. Zero distance corresponds to aggregated NPs that were prepared by adding acetone into the NP suspension in a 1:1 proportion. Maximal distance corresponds to the case where one to a few NPs occupy the whole irradiated volume. The dependence of the PTB generation threshold upon the interparticle distance (Figure 7B) showed a maximal level of 37 J/cm^2, which has a plateau for the distances above 6 μm. It also showed almost exponential behavior at shorter distances, decreasing almost by 20-times from 37 J/cm^2 to 1.8 J/cm^2 with a minimum of 0.76 J/cm^2 (almost 50-times lower than that for single NPs at long distances). In the case of NP clusters, the PTB lifetime (which characterizes its maximal diameter) was found to be 13 ± 3 ns (at a fluence of 2.8 J/cm^2) and did not depend upon interparticle distance, except for the cluster case. PTBs around NP clusters yielded a much longer average lifetime of 249 ± 164 ns (same laser pulse fluence), which indicated that the maximal diameter of the PTBs around clusters of NPs was 19-times bigger than that for single NPs. In addition, the PTBs around single NPs were not reproducible during the next laser pulses but were sometimes reproducible around clusters of NPs.

The obtained results can be explained by the action of different mechanisms of PTB generation, dependant on the interparticle distance. Distances above 8 μm isolate the NPs thermally so that the PTBs are generated around single NPs and therefore the threshold does not depend upon the interparticle distance and NP concentration. At shorter distances the enhancements of mutually overlapping thermal fields around the NPs may decrease the PTB generation threshold temperature of the individual NPs and hence the laser fluence threshold. Also, it

should be understood that the PTBs that we are considering are hydrodynamic phenomena that develop after the bubble vapor nucleus overcomes the limiting action of the surface tension. This threshold (considered by us as the PTB generation threshold) for the NPs, with their small radii, is significantly higher than the threshold for formation of the vapor nucleus around NPs. The latter may be estimated as the laser fluence required to heat the NP surface above 100°C (boiling temperature) and is in the range 0.005–0.02 J/cm^2. However, overcoming the surface tension barrier requires much higher fluence, in the range 0.012–0.5 J/cm^2, as was experimentally shown.

PT properties of gold NPs under high optical energies

Photothermal bubble generation around gold NPs implies that the initial laser-induced temperature of the NPs can be very high and may potentially exceed the melting and even evaporation thresholds for gold. The irreproducible nature of the NP-generated PTBs indirectly confirms this assumption. Therefore, the plasmon interactions (which are responsible for heat generation by the NPs) during the generation of the PTBs may be significantly influenced by high-temperature effects in the NP: melting, shape transition and disintegration. To estimate the high-temperature efficacy of the plasmon resonance mechanism for the generation of the PTB we have measured and compared PTB lifetimes and threshold fluences for three types of NP: 30 nm NSPs, 14 × 45 nm NRs and 170 nm silica–gold NSs. Two laser pulse (10 ns single pulse) wavelengths were applied: 532 nm is close to the transverse resonance wavelength for NRs and also an off-resonant wavelength for NS, and 750 nm is close to longitudinal (the main plasmon band) resonance wavelength for NRs and for the plasmon resonance wavelength of NSs (Table 2 & Figure 8).

The most unexpected result for the NPs with near-infrared plasmon resonances (NRs and NSs) was that PTB lifetimes were much longer at 532 nm rather than at resonant wavelengths of 750 nm (Figure 8). In addition, the thresholds of PTB generation were found to be significantly lower for the nonresonant wavelengths (Table 2). Furthermore, at certain fluence ranges (for NSs this is 0.1–0.2 J/cm^2, for NRs this is 10–20 J/cm^2) PTBs were generated at 532 nm but were not generated at 750 nm. These results are opposite to the ‘cold’ optical properties of these NPs: nonresonant optical absorbances of NRs and NSs were lower than those at the resonant wavelengths, which implies that these NPs should emit much less heat at 532 nm and much more heat at 750 nm (Table 2). Therefore, we concluded that at high excitation optical energies the specific plasmon bands of the NRs and NSs were tremendously suppressed and their ability to generate PTBs was decreased by 16–23-times (relative to that at nonresonant wavelength of 532 nm). From the practical point of view it turns out that the visible (532 nm) and non-resonant excitation of NPs is more efficient at high fluences rather than ‘traditional’ excitation at the wavelengths matching the near-infrared plasmon bands. This effect requires further investigation and can be explained by the damage of the NPs during their interaction with the pump laser pulse.

We may conclude from the described experiments that the mechanisms and thresholds of generation of PTBs around light-absorbing NPs significantly depend upon interparticle distance between the NPs, and particle diameter. Maximal thresholds were found for isolated small NPs and minimal thresholds corresponded to big and closely located NPs. Additional details can be found in [28,29,54,55].

NP-generated PTBs versus PTBs in micro- & macro-samples

In our next experiment we compared the NP-generated PTBs with the PTBs generated in uniformly absorbing micro- and macro-samples: red blood cells as the microabsorber and in the solution of hemoglobin as the homogeneous absorber. The influence of the pulse length was similar to that found earlier for gold NPs, although the increase in the PTB generation

threshold fluence for a 10-ns pulse was smaller than that in the case of NPs: for the red blood cells it was 8.4-times and for the homogeneous solution of hemoglobin it was only 2.9-times (Figure 6) . The most important difference between the PTB generation around plasmonic NPs and homogenous absorbing media has been described above as the ‘thermal insulation’ effect for the NP-generated PTBs. We have summarized in Table 3 the differences in PTB generation mechanisms at nano- and micro-scales.

The difference of PTB generation mechanisms can be explained through the size of the heated volume, which is determined by the size of the heat source and by the thermal diffusion radius:

$$R_t=(24a\tau_l)^{\frac{1}{2}}$$

that depends upon the pump pulse duration. In homogeneous media and for a relatively short laser pulse the size of the heat source is determined by the diameter of the pump pulse (7000 nm) because R_t is much smaller. Thus the heated volume of the homogeneous absorber is determined only by the laser beam aperture. When NPs act as the heat sources in transparent media the volume of the heated media is determined by that of the NPs and by the thermal diffusion radius. Thus, the heated volume of the media around NPs:

$$V_h(NP) \approx \frac{4}{3\pi}([0.5D_{np}+\{24a\tau_l\}^{\frac{1}{2}}]^3 - \frac{D_{np}^3}{8})$$

depends mainly upon the pulse duration. For our experimental conditions the NP-heated volume is six–eight orders of magnitude smaller than the laser-heated volume in the homogeneous absorber. Therefore, the spatial scale of thermal processes in homogenous media and in microabsorbers is determined by the size of the optical absorber or by the laser beam aperture, while for nanoabsorbers the spatial scale of thermal processes is determined by the duration of the laser pulse. In additon, for nanoabsorbers, the longer the laser pulse, the lower the laser-induced temperature and the more optical energy is required to reach the vaporization temperature threshold. This explains the difference in PTB-generation threshold fluences for plasmonic NPs for laser pulses of the two different durations (10 ns and 0.5 ns). Also, our result is in line with the concept of selective laser-induced heating of biotargets [62]. However, further decrease of laser pulse duration down to pico- and femto-seconds will not improve PTB generation conditions because too-long pulses would generate not only PTBs but also pressure and shock waves (Figure 2) [22,23,34,63–69]. We did not observe pressure waves in our experiments with 0.5 ns and 10 ns pump pulses (in [18] the shock waves were detected for a 30 ps pump pulse with a similar technique). A pulse length of 0.5 ns is long enough to avoid significant pressure build-up in the NPs and thus no strong pressure waves should be expected.

Nonreproducible PTBs may imply melting of the NPs, which practically turns off the plasmonic mechanism of energy conversion. This corresponds to the temperature of gold melting (1337 K). Reproducible PTBs that were detected at fluence levels close to the PTB generation threshold may imply a minimal temperature level in the range 370–500 K (for normal pressure). These numbers estimate the initial laser-induced temperature of the media around the NPs. Heat transfer models for low laser-induced temperatures in the range well below the melting threshold show that heat is transferred within 100–300 ps from the NP into the nanoenvironment [15,46,68,69]. More precise estimation requires reliable data on actual values (and dynamics) of optical absorption cross-sections of the NPs in high-temperature ranges, including NP melting. Current models [69–71] use the absorption cross-section as the constant, which is not true: it was shown by Otter in 1961 that optical absorbance of the gold significantly deteriorates (by more than one order of magnitude) as the temperature approaches the melting

threshold, and more recent works have demonstrated temperature dependence of the absorbance cross-section of plasmonic NPs [44,72–76]. Recently, we have experimentally shown that at high laser-induced temperature the behavior of plasmon resonances and PT efficacy of gold NPs significantly differ from that at lower temperature [29].

The maximal diameter of the PTBs can be estimated through measurement of the PTB lifetime, through available models of bubble dynamics [20,22,47–50] and through experimental data on micrometer-sized bubbles, whose diameters were directly correlated to their lifetimes [23, 47,66,77]. Maximal diameter of the PTBs generated around 35 nm gold NPs in water was reported to be 250 nm [24,25,70,78]. In cited works the laser-induced fragmentation of gold NPs was also detected and this explains the poor reproducibility of the PTBs in our experiments. Therefore, we may estimate the maximal diameter of the PTBs to be 200–400 nm (for 30 nm gold NSPs, based on the data from [26]).

Our results show that the parameters of NP-generated PTBs depend upon many factors related to laser pulse, NP size, shape and aggregation state, and even upon sample chamber. We may conclude that optimal duration of the laser pulse (in the subnanosecond range) and clustering of the NPs provide the most efficient and controllable generation of PTBs at the lowest threshold fluence. The lifetime and size of PTBs can be varied with the level of laser fluence. Described previously the optical, thermal and mechanical properties of PTBs may be employed in different biomedical technologies so as to improve their sensitivity, efficacy, selectivity and safety. Additional details can be found in [28,29,54–56,79,80].

Biomedical properties of gold NP-generated PTBs

Gold NP interaction with living cells: clustering & toxicity

We have studied the internalization mechanisms of gold NP with five techniques: fluorescence microscopy, fluorescence flow cytometry, optical scattering, atomic force and scanning electron microscopy (SEM). We have employed 30-nm gold NSPs because this size is big enough to generate thermal energy and small enough to allow internalization (objects with sizes bigger than 100 nm can hardly enter the cell cytoplasm [52,81]). Gold NPs do not emit light, so they were tagged with phycoerythrine fluorescent dye for optical fluorescent detection. We used a suspension of living cancer (leukemia) cells K562 as a model. We applied several targeting approaches, such as:

- NP functionalization state: bare NPs and NPs preconjugated with cell-specific monoclonal antibody CD33;
- Incubation temperature: 4°C to allow only antibody–receptor interaction and to surpress physiological processes and 37°C to allow physiological processes;
- Incubation time: from 15 to 120 min so as to monitor the accumulation of NPs in the cells and NP toxicity.

First, we applied targeting that was based on antibody–receptor interactions so as to analyze the accumulation of NPs at the cellular outer membrane. Comparison of the images for the intact (Figure 9, left panel) and NP-treated cells (Figure 9, center panel) has revealed NP-related signals in 90–95% of targeted cells and with highly heterogeneous spatial distribution of NP-related signals within the cell. The NPs were detected as highly localized signals and atomic and electron microscopy have directly shown the clusters of closely aggregated NPs. Combined application of SEM and spatially-resolved energy-dispersed spectroscopy (spatial resolution is 100 nm) confirmed that local bright structures at the cell membrane (Figure 9A, middle) contain gold, with the mass being much higher than the mass of a single NP. Therefore, we believe that the detected structures represent gold NP clusters. Optical methods also yielded localized NP-related signals in targeted cells (Figures 9C–9E). These signals were much

stronger in pixel image amplitude than those obtained from untreated control cells (Table 4). Amplitudes of the fluorescent and scattering signals were five-times higher than those for untreated cells presented in Figures 9C & 9D (left panels). The size of the NP clusters was in the range 100–300 nm, and thus the diameter of the NP clusters that were formed at the cellular membrane was three–ten-times bigger than the diameter of the single NPs. We did not find NP-related signals on the images of control cells.

Next, we analyzed the influence of temperature and time of the incubation of cells with NPs. Physiological temperature (37°C) activated endocytosis in the cells and this resulted in the appearance of bigger NP clusters in the cytoplasm. In K562 cells, NP-related signals increased (see Figure 9 [right panel] and Table 4) from 564 to 832 counts (fluorescent microscopy), from 3450 to 9200 counts (optical scattering microscopy), and according to SEM, the maximal diameter of detected NP clusters increased from 300 to 800 nm.

Internalization of the NPs was directly registered with SEM and atomic force microscopies (see Figure 9A [right panel]). Thus, the electron and atomic force microscopies have directly showed that the NPs and their clusters were internalized by the cells within 30–120 min. It should be noted that NP-related signals were never observed in the nuclei area of the cells. It appears that NPs cannot penetrate through the nuclear membrane. The results obtained for cells incubated at 37°C allow one to conclude that during this incubation NPs and small NP clusters disappear from the cell membrane and appear in the cellular cytoplasm as large NP clusters. The biological mechanism responsible for the above-described processes is endocytosis. Low temperatures (e.g., 4°C) disable endocytosis and, therefore, during the incubation of cells with NPs at 4°C no NP internalization occurs. Similar results (coupling to cell membrane, internalization into cytoplasm and concentration into endosomes) were obtained earlier [82], although the clusters of the NP were not defined as specific nanostructures.

Similar results were obtained during a study of gold NR uptake by Hep-2C cells that over-express EGF receptor (EGFR). Highly localized signals were detected in the Hep-2C cells after their incubation with the NR-C225 (C225 is an antibody against EGFR). The amplitudes of optical scattering signals for Hep-2C cells were found to be 547.3 ± 195.0 counts for intact control cells and 2766.7 ± 907.4 counts for NR-treated cells, as population-averaged values. The small size of NRs means that we can assume that they penetrated through the outer cellular membrane via endocytosis and then were concentrated into clusters.

Nanoparticle safety is the subject of massive studies and was reviewed in [1,2,83]. Among all NPs, gold ones were found to be the safest [1] and are FDA approved. We experimentally monitored the viability of cells after their interaction with the gold NSPs by using propidium iodide (PI) dye (which penetrates through the damaged membrane and thus stains the dead cells) and flow cytometry. Incubation at 4°C did not have any considerable negative effect on the cells. For K562 cells the level of PI-positive cells changed from 2% before targeting to 2.8% after targeting. Incubation at 37°C resulted in additional damage to the cells, increasing the level of PI-positive cells up to 3.4%. Nevertheless, these values indicate that targeting cells with NPs and the processes of NP clustering are relatively safe. This is partly due to the nontoxic nature of gold NPs, which have been shown to have negligible toxicity on living cells [1,2, 83]. The viability of the cells after their incubation with NRs was measured with the trypan blue exclusion test. Initial viability of the cells prior to their incubation with NRs was 95% ± 3%. After incubation with NR-C225 for 30 min the viability of the cells was found to be in the range 80% ± 10%. The viability of the control intact cells also slightly decreased to 89% ± 4%. The conjugates of NR-C225 were not absolutely safe for the cells. Their toxicity can be caused by minor amounts of residual cetyl trimethylammonium bromide (CTAB) molecules that might be left on NRs after their conjugation with the monoclonal antibody. Currently, there are almost opposite points of view on the cytotoxicity of NRs with CTAB: some groups have reported

that CTAB does not influence the viability of the cells [84–86], while the others found a strong cytotoxic effect of CTAB [87,88]. We consider that CTAB should not be used, even in minor quantities, owing to its toxicity.

Therefore, we may conclude that the interaction of bare and functionalized NPs with living cells as a rule creates clusters of many closely located NPs that are linked through specific antibodies and/or by cellular structures, such as endosomes and vacuoles. Advantages of clusters over single NPs for medical diagnostics and therapy using optical methods include a much greater volume, which allows effective PT interactions under conditions of relatively slow heat diffusion. Formation of clusters does not compromise viability of the cells. Additional details can be found in [51,53,58,89,90].

Gold NP-generated PTBs in living cells

Generation of PTBs in living cells (carcinoma cell line A549, Hep2C, leukemia cells K562) was studied *in vitro* for several types of gold NPs: NRs with the dimensions 13.6 × 45.9 nm, 39.5-nm NSPs and silica/gold NSs with a diameter of 50 and 171 nm. According to optical extinction spectra of the suspensions of these NPs the pump laser wavelengths were chosen to match the maxima of optical absorbance for each type of NP (Table 2). It should be noted that clustering of the NPs did not significantly shift their peaks and therefore we have used the same pump laser wavelengths for NPs and NP clusters. Pump and probe laser beams were focused on a specific cell that was positioned manually with a microscope stage into the center of the laser beams. Each cell was exposed to a single pump pulse. In this study we have applied the PT microscope previously developed by us for generating and detecting PTBs in individual cells [79]. Each cell was illuminated with three collinearly focused laser beams: 10 ns pulsed pump beam for the PTB generation (532 nm or 720–840 nm), and two low-intensity continuous (633 nm, 0.1 mW) and pulsed (10 ns, 750 nm) probe beams for detecting PTBs in real time (see experimental section for details). Two optical signals were obtained simultaneously during the laser pulse: the time response from the whole cell (Figure 10A & B) and time-resolved (with 20 ns delay to pump pulse) optical scattering image (Figure 11). This allowed us to detect and measure PTBs in the cell. PTBs were identified according to time responses of negative and symmetrical shapes that are specific to PTBs (Figure 4) and were also detected in time-resolved images. Peripheral location of the PTB-specific signals in the time-resolved images of the cell (Figure 11A) show that the PTBs were generated in the cytoplasm and presumably not in the nuclei. Increased fluence of the pump laser pulse caused an increase of the PTB diameter (Figure 11B). For all types of employed gold NPs the PTB responses did not show any detectible residual environmental heating after PTB termination (Figures 10A & 10B). This means that the temperature outside the PTB did not increase relative to the ambient level and thus the NP-generated PTBs induce mainly mechanical, not thermal, impacts in the cells and outside the PTBs. The mechanism of cell damage due to PTBs is discussed later.

We have compared NP-generated PTBs in living cells with the PTBs generated in the intact cells due to optical absorbance and heating of endogenous cellular chromophores (in most cases and for visible laser wavelengths these are the hem-containing molecules such as cytochromes and hemoglobin). The PTB response registered from the intact lymphocyte cell (Figure 10C) differs from the responses of the NP-generated PTBs: at the very beginning of the PTB and after its collapse it shows clear signs of increased temperature of the media (a short positive peak in front of the PTB dip and a positive deviation of the signal from the base level after the PTB termination that gradually returns to the base level due to cooling of the bulk media). The obtained response represents the superposition of PTB and thermal signals (similar to Figure 4D). The process of the generation of PTBs around cellular endogenous optical absorbers is similar to PTB generation around microabsorbers and in homogeneous media, where PTB generation is accompanied by the bulk heating of the environment and

therefore the PTB delivers not only a mechanical impact (as in the case of NP-generated PTBs) but also a thermal one. Also, the cell-generated PTBs were not reproducible: exposure to the second laser pulse yielded no PTB, possibly due to photo- and thermal damage of cellular optical absorbing structures.

Photothermal bubble generation probability *PRB* was measured at several pump pulse fluence levels so as to cover the range from those close to zero (no PTB) to those close to one (PTBs were generated in 100% of the cells). As the laser fluence increased, the *PRB* values gradually increased from 0 to 1 and the monotonous character of the *PRB*(ε) dependence was found to be typical for all studied cells and NPs. Obtained dependences of *PRB*(ε) (not shown) were used to determine laser fluence thresholds for PTB generation (Table 5). We have found that PTB threshold levels for C225-positive cells were lowest when NS–C225 conjugates were applied. Incubation of the same cells with bare, nonconjugated NSs resulted in a 22-fold higher threshold, which coincided with that measured for the water suspension of nonaggregated NSs. In addition, we have incubated EGFR-negative cells, the lymphocytes, with NS–C225 conjugates. The PTB-generation threshold in this case was found to be very close to that obtained for the water suspension of nonaggregated NSs (Table 5). This means that single NSs might occasionally get into the nontarget cells, although they did not form NP clusters. The PTB generation thresholds for different intact tumor cells that were not incubated with NSs and were used as additional controls were significantly higher (Table 5). The difference between PTB generation thresholds for the intact cells and those treated with gold NSs reached almost two orders of magnitude. The lifetimes of PTBs obtained for A549 tumor cells (Table 6) are comparable to the lifetimes obtained for NP clusters in suspensions and are significantly longer than the lifetimes obtained for suspensions of single NPs. This also directly indicates that the sources for intracellular PTBs were NP clusters in cells, not single NPs. Comparing the tumor cells targeted with NS–C225 conjugates and intact nontargeted cells, we may conclude that the application of the tumor-specific gold conjugates and the formation of NP clusters has decreased the laser fluence threshold in tumor cells by almost 100-times (Table 5).

We also studied the lifetime of PTBs generated around NRs and NR clusters and in NR-treated cells as a function of laser pulse fluence (Figure 5B). The increase in PTB lifetime with the increase in laser fluence is in line with the basic thermodynamics of PTB generation: the more optical energy is deposited into NRs, the more thermal energy is produced and this increases the maximal diameter of the PTB and its lifetime. Comparison of the three curves obtained for the suspension of single NRs, NR clusters and the curve obtained for the cells treated with the same NRs shows that cell-related PTBs were much closer in their lifetimes to those generated around NR clusters than single NRs (Figure 5B). In the cells, the PTB generation threshold decreased by 40–100-times and the PTB lifetime (and, hence, the maximal diameter of the PTB) increased by 30–40-times relative to the NR suspension. Therefore, we have received several experimental and independent proofs that not single NRs, but NR clusters are the source of PTBs in cells. The former did not produce any PTBs at the decreased laser fluence levels that were applied to the cells.

We suggest that efficient clustering of small NPs (that easily underwent endocytosis by the cells and were then concentrated in the endosomes into clusters) provided a bigger PTB than the application of big NPs, whose uptake by the cells is biologically limited. The next cluster-specific result is that NP clusters survived the laser pulse and were able to generate PTBs during the exposure of the cells to up to 100 pulses. This feature was not applicable to the suspension of single NPs in water, nor did we detect follow-up PTBs while exposing NP-treated lymphocytes with several laser pulses. This means that single nonclustered NPs were damaged with a single laser pulse and, therefore, cannot absorb follow-up laser pulses.

The threshold laser fluence of PTB generation in the intact cells was one–two orders of magnitude higher (20–50 J/cm^2) compared with the PTB threshold fluence of the NP-treated cells (especially for those with NP clusters). Also, lifetimes of PTBs in the intact cells were longer (400–600 ns) than those for NP-generated PTBs. High thresholds and long lifetimes of such PTBs imply that their sources are significantly bigger than the NPs and their clusters and also have a much lower optical absorbance than that of gold NPs. Thus the NP-mediated generation of PTBs in living cells is a highly selective process because no other PTBs can be generated in the cell at such low fluence levels and the NP-generated PTBs do not deliver an additional thermal load to the cellular microenvironment.

The influence of the kinetics of NP accumulation on the PTB generation threshold fluence and lifetime was studied by monitoring the interaction of the bare 30-nm gold NSPs with K562 leukemia cells *in vitro*. Living K562 cells were incubated with bare 30-nm gold NSPs for 0 (control sample), 15, 30 and 60 min at 37°C. After incubation was completed, unbound NPs were washed off after centrifugation, cells were fixed with 10% para-formaldehyde solution and were analyzed with PT microscopy (the most sensitive method). As NP cluster-related parameters we measured the threshold and lifetime of laser-induced PTBs as a function of incubation time (Figure 12). Those parameters are the most cluster-specific and do not depend upon endocytosis like the fluorescence intensity described earlier.

We have found that after 15 min of incubation, the NPs aggregated into clusters. At this stage the threshold of PTB generation in cells (13 J/cm^2) was three-times lower than the PTB generation threshold around individual 30-nm gold NSPs (37 J/cm^2). This difference in threshold levels means that PTBs were generated around NP clusters that are significantly bigger than single NPs. Analysis of the PTB lifetimes confirmed this conclusion. At the laser fluence level of 8 J/cm^2 no bubbles were detected from single NPs, but bubbles were detected in the cells. Further incubation for 30 min resulted in a substantial increase in bubble lifetime and decreased bubble generation threshold. Longer incubation of the cells with NPs did not produce significant changes in NP cluster-related parameters (Figure 12), which may indicate saturation of the internalization processes. The large spread in PTB lifetimes as indicated by the error bars in Figure 12B reflects the heterogeneity of cell properties in one population. This means that younger and older cells may have different endocytosis activity, and thus NP clusters formed in these cells may vary in their diameters. As a result, the bubbles around such NP clusters will be of different diameters, and measured lifetimes will also be very different.

This experiment confirmed that the aggregation of NPs into clusters occurs even when bare NPs without monoclonal antibody are used and such clustering is provided by endocytosis – a natural physiological process. NP cluster formation due to endocytosis is quite fast and almost completes in 30 min at physiological temperature. Additional details regarding the experiments reported above can be found in [38,53,57,80,89–97].

Cell damage by PTBs

The influence of NP-generated PTBs on cell viability was evaluated optically with two standard microscopy techniques that monitor the integrity of the cellular outer membrane [98]. First, a white light transmittal image was obtained for the cell before and after its exposure to pump pulse and the difference of these two images was used to detect any PTB-induced changes to the shape of the cell. Second, the cell damage by PTBs was detected using a standard fluorescent method by monitoring the cellular uptake of ethidium bromide dye. Prior to the experiment, ethidium bromide dye was added to the cell samples. This dye penetrates the membranes of compromised cells and produces red fluorescence upon excitation with a light source. Contrarily, this dye does not penetrate the membranes of living cells and hence produces no fluorescence for living cells. We have used, for excitation of the fluorescence, a single laser pulse (532 nm) with the fluence decreased by 20-times relative to the PTB generation level.

Fluorescent images were obtained for each A549 cell before and after PTB generation. Their pixel amplitude ratio was used to quantify the damage.

The images (Figure 13) and Table 6 show the data for the two A549 living cells that were treated with 170-nm gold NSs and then were exposed to single pump pulses (10 ns, 532 nm) with the fluences 0.64 J/cm^2 (cell 1, top panel of Figure 13) and 0.48 J/cm^2 (cell 2, bottom panel of Figure 13). According to the scattering images (Figure 13C) and corresponding PT responses (not shown) both cells have yielded intracellular PTBs of sub-μm size and with PTB durations of 250 ns for cell 2 and 70 ns for cell 1. Under given fluence levels these two cells yielded only a single PTB around the biggest NS clusters. According to the fluorescent and white light images of the two cells shown in Figure 13, the cell 1 has been damaged, while the cell 2 has survived the PTBs generated in them. Based on the differences in the optical scattering amplitudes and the lifetimes of the PTBs in these two cells (both parameters were much higher for the damaged cell), we address the damaging effect to the maximal diameter of the PTB. In addition, both cells' responses did not indicate any residual bulk heating after the collapse of the PTBs.

In another experiment, Hep2C cells (overexpressing EGF) were targeted with 50-nm gold NS–C225 conjugates and were then exposed to single 10-ns laser pulses at 750 nm. The viability of cells that yielded PTBs was analyzed as described above. Instead of ethidium bromide dye, trypan blue dye was applied. After the single pulse-generated PTBs the cells exhibited apparent changes to their shape, were positively stained and thus were considered to be damaged. The lifetime of the detected PTBs was above 100 ns.

Based on the obtained results (the detected damage to the cell membrane, the absence of laser-induced heating of the bulk area, the single pulse effect and almost immediate cell damage) we suggest that the mechanism of cell damage is associated with the mechanical, not thermal, impact of the expanding and collapsing PTB. Such mechanical destruction of the cellular membrane and possibly of some other components such as the cellular skeleton may cause rapid and irreversible blebbing and lysis of the cell. This mechanism is in line with the available independent experimental data on cell damage with ultrasound-induced extracellular bubbles [30,31,34,36,37,97–106] and with recently reported results where NRs were targeted to tumor cells and then excited with femtosecond laser pulses, causing blebbing of the targeted cell [7]. The mechanism of cell damage in our experiments differs from the most recognized PT mechanisms [8,16,107–111], which imply excessive heating above thermal damage thresholds. In the case of NP-generated PTBs it may be possible that all NP-generated heat is confined by the PTB and does not spread outside.

Analysis of the collateral cells where no bubbles were detected has shown that such cells were not damaged after the laser pulse (data not shown). This result also proves the spatially and temporally limited nature of thermal processes in PTBs: their maximal size being 10–20 μm and their lifetime being within 1 μs, they do not reach other cells. Therefore, the NP–PTB mechanism may provide a much better selectivity compared with other PT mechanisms that employ laser-induced heating mediated through light-absorbing NPs. To achieve the NP-induced temperatures sufficient for cell damage in the volume of the whole cell, the exposure time (pulse duration) should be much longer than nanoseconds and this causes the spread of the laser-induced temperature far outside the target cell. The reported exposure times vary from 100 μs to minutes [10,16,109–111] meaning that thermal diffusion will be in the millimeter range and all cells within this range will be influenced – target and normal cells. The same rule can be applied to diagnostic PT methods: single cell sensitivity can be achieved with the event, which can be spatially localized within one cell and will not spread over a larger population.

The above-mentioned selectivity of cell damage is based on the use of three components that are specific for PTB generation in NP-targeted cells: clusters of NPs instead of single NPs, a short laser pulse instead of a long pulse or continuous irradiation, and PTBs instead of heating as a damaging process. This improved selectivity may be the key to future safety and efficacy of clinical applications. The idea of using a short laser pulse to localize the thermal effect of laser irradiation is not new and was introduced almost 20 years ago by Anderson and Parrish [62]. Later, this group also demonstrated the damaging effect of the bubbles generated around gold NPs [8]. Proposed by us, the cluster–bubble mechanism is the next step in the development of improved spatio-temporal selectivity of PT biomedical methods. Additional details can be found in [38,53,57,89,[90],[92],93,95,112,113].

PTBs as optical probes

Amplification of optical scattering by PTBs—Optical scattering has been used for sensing vapor and air bubbles of macro-size [26,34,67]. Laser-induced PTBs of small sizes generated around NPs and their clusters may also be used for the optical imaging of specific targets (such as cells or molecules) associated with plasmonic NPs. Metal NPs have excellent scattering properties that have been employed in various bioimaging applications [3–6]. However, the challenge of NP scattering imaging is in the strong background scattering by cells and tissues, which limits the sensitivity of NP-based imaging techniques. PTBs may amplify optical scattering signals by 100–1000-times relative to that of gold NPs due to their increased diameter (relative to that of NPs), because the intensity of optical scattering increases with the increase of probe size by the diameter to the sixth power [37]. A highly sensitive imaging method (Figure 14) employs two laser pulses: a pump pulse to generate the PTB around the target-linked NP and a probe pulse to illuminate the PTB.

The mechanism of optical amplification is universal and depends upon the PT properties of gold NPs (as PTB sources) and upon the pump and probe laser parameters. Thus, PTBs can be considered as a new type of optical sensor that can be selectively activated ‘on demand’ around plasmonic NPs coupled to specific targets. Clustering of small NPs inside the cell further increases the scattering amplification and overrides the biological limitation on the maximum diameter of NPs for intracellular delivery. Optical scattering can be detected from a zero level when the light scattered by a PTB in a specific direction is registered, thus producing a positive signal that characterizes an angle-specific scattering effect. Alternatively, the probe beam can be directed into the sensor so that the scattering in all directions by the PTB decreases the amount of light at the detector, thus producing the negative signal that characterizes the integral scattering effect. Also, besides the pulsed probe beam, continuous illumination and detection can be used to register the kinetic behavior of the scattering signal. We defined continuous optical monitoring of the PTB as a response mode and time-resolved pulsed imaging of the PTB as an image mode. Image and response modes can be used simultaneously, thus combining PTB imaging and a measurement of its lifetime. The threshold nature of the PTB implies better contrast and signal-to-noise ratio compared with conventional nonthreshold techniques that employ fluorescent and scattering probes (including gold NPs). Two described PTB sensing techniques have different properties that are summarized in Table 7.

Scattering properties of PTBs were analyzed for nonclustered and clustered 30-nm gold NSPs. We exposed the sample with 30-nm gold NSPs to single pump laser pulses of 0.5 ns duration at gradually increasing fluence levels. All samples were studied in cuvettes with a diameter of 9 mm and height of 10 μm. Optical scattering images were obtained prior to pump pulse (Figure 3A & C) and at a specific time delay (9 ns) after the pump pulse (Figure 3B & D). Without the pump pulse, the scattering from single NPs was too weak to form detectable images of single NPs. However, application of single pump laser pulses at fluence starting from 0.5–0.6 J/cm^2 resulted in the appearance of bright diffraction-limited spots in the images. Unlike the

single NPs, their clusters scattered the probe pulse more strongly and formed images (Figure 3C). Increased optical scattering by NP clusters compared with that of single NPs was caused by their increased size, estimated at 400–500 nm with transilluminated imaging. Application of the single pump laser pulse caused bright spots in scattering images (Figure 3D) that spatially coincided with NP clusters. Pixel amplitudes of the images and the lifetime of cluster-generated PTBs were found to be significantly higher, and the threshold fluence of bubble generation significantly decreased compared with those for single NPs (Table 1). As can be seen from Figure 3 the bubbles have amplified optical scattering. This effect was characterized through the relative scattering amplitude (Table 1). The amplification effect was also stronger for the NP clusters than for single 30-nm NPs. Significant increase of the responses duration of cluster-generated PTBs (Table 1) relative to that of single NPs implies an increase of the maximal diameter of cluster-generated PTBs and so explains better optical amplification, because optical scattering is very sensitive to the size of the scattering object. Additional details can be found in [55,56].

PTB scattering imaging of living cells—The imaging potential of PTBs was evaluated for A549 (carcinoma) cells incubated with 170-nm NSs. Side-scattering images were obtained for individual living cells before and during the pump with a time-delayed pulsed probe pulse (750 nm, 10 ns). The first image was formed mainly owing to the scattering by intracellular NSs or NS clusters. The second image was registered with 20 ns time delay and was used for PTB detection. Pixel amplitudes of the PTB image were normalized by the pixel amplitudes of the NP image obtained for the same cells and the resulting amplitude of the ratio image (K_{ssc}) was considered as the scattering amplification coefficient:

$$K_{SSC} = \frac{A_{PTB} - B}{A_{cl} - B}$$

where A_{PTB} and A_{cl} are the pixel image amplitudes obtained for the same cell in pulsed scattering mode for the PTB (pump laser on) and NSs (pump laser off), respectively, and B is the constant for the background amplitude (which also counted for the scattering by cellular structures). Influence of the PTBs on the optical scattering signal is illustrated in Figure 13. The images show two A549 living cells that were exposed to single pump pulses with the fluences 0.64 J/cm^2 (cell 1, top panel of Figure 13) and 0.48 J/cm^2 (cell 2, bottom panel of Figure 13), respectively. According to the scattering images (Figure 13C) and corresponding PT responses both cells have yielded intracellular PTBs of sub-μm size and with PTB durations of 250 ns for cell 2 and 70 ns for cell 1. Both cells yielded only single PTBs, which can be explained by a relatively inefficient nonspecific endocytosis of 170-nm NSs by these cells. In general we have observed up to eight–ten PTBs in individual cells and their number increased when pump laser fluence was increased. Laser-induced PTBs (Figure 13C) have caused an increase in optical scattering by almost three orders of magnitude (Table 6) relative to the scattering of gold NSs at the same point of the image (Figure 13B). Specifically, the amplification coefficient at the higher laser fluence (top cell 1 in Figure 13) was 2886, while at the lower laser fluence (bottom cell 2 in Figure 13) it reached 1779. Analysis of fluorescent and white light images has shown that the cell 1 was damaged by the PTB because its fluorescence has increased (Figure 13D; top) and its shape significantly changed (Figure 13E; top). Under the lower pump laser fluence cell 2 has survived the pump pulse and PTB: no increase of the fluorescence (Figure 13D; bottom) and no change in the cell shape (Figure 13E; bottom) were detected. PTB lifetime in surviving cells was shorter than that for damaged cells and this difference shows that the maximal diameter of the PTB in surviving cells was smaller than that for damaged cells.

Next we incubated the A549 cancer cells with gold NSPs of 30-nm diameter and with gold NS of 170-nm diameter and compared the optical amplification effect of the PTB. We found that under equal pump laser fluences the amplification of optical scattering in both samples was similar despite the significant differences in the scattering properties of small NSPs and big NSs that were used (Figure 15). Amplification coefficient was found to depend upon PTB lifetime, which, in turn, was increased through the controllable increase of the laser pulse fluence. It should be noted that the big diameter of gold NSs (170 nm) might not improve the scattering due to poor internalization (and hence clustering) of such big NPs by the cell. We may assume that bubble size, not NP size, is important for the amplification of optical scattering. These results have demonstrated proof of principle for PTB imaging: the cluster–bubble mechanism has provided amplification of optical scattering in living cells by more than 1000-times (compared with scattering by gold NPs) and without damage to the cell. Therefore, NP-generated intracellular PTBs may be considered as noninvasive and highly sensitive optical probes.

When PTBs are generated in living cells the viability becomes the most significant factor and the parameters of the bubble and laser radiation should be below the cell damage thresholds. Generation of laser- and ultrasound-induced bubbles has already been studied in terms of the mechanical damage of cell outer membranes. It was found that a cell may repair its membrane if the maximal diameter of the bubble does not exceed 1–2 μm. Optical scattering of the vapor bubble of 1-μm diameter is several orders of magnitude stronger than optical scattering from gold NPs that can be delivered into the cells (see Figure 3). The size of the bubble image (up to 1 μm) may exceed the actual size of the target (the latter may have a nanometer size that is well below the diffraction limit), but the bubble would definitely help to detect the presence of such a target as the single molecule in a specific cell. NP-generated PTBs, unlike the fluorescent probes, do not exist in the cell until after they are generated, and the gold NPs that are present in the cell are much less toxic than any fluorescent probes. Therefore, the influence of PTB imaging on cell physiological processes can be minimized. The threshold mechanism of bubble generation provides selectivity of optical signal and thus increases signal-to-noise ratio of imaging. Bubbles can be activated with specific wavelength and energy of laser pulses and otherwise they do not emerge in a cell, so they would not interfere with cellular processes or with other measurements. Additional details can be found in [38].

PTB cytometry—The specificity and sensitivity of the PTB scattering method were evaluated by comparing the PTB and NP scattering signals obtained from three different cancer cells. We targeted K562 leukemia cells and carcinoma cells A549 and Hep-2C with 30-nm gold NSPs, and analyzed the amplitudes of the integral side-scattered signals from individual cells. The signals were obtained for intact, NP-treated, and NP- and pump laser-treated cells. Generation of PTBs in each individual cell was simultaneously and independently monitored by registering PTB response to ensure that the PTB was generated. Each cell was exposed to a single pump pulse and two scattering signals were obtained: the first signal registered before exposure to pump pulse characterized integral optical scattering from the NPs and their clusters in the cell (x-axis of Figure 16), while the second signal registered during the pump pulse and after it has characterized the PTB generated in the cell (y-axis of Figure 16). These two scattering signals were plotted in a diagram where each dot represents an individual cell (Figure 16). This diagram shows a distinct line for ‘no bubble’ cases. All dots that are above this line correspond to PTBs. According to the results obtained for all three types of cell, the NPs amplify the scattering but not significantly relative to the scattering by intact cells. PTBs provided a significant increase of the amplitudes of scattered signals in all studied cells (Figure 16; y-axis). The amplification factors were calculated by normalizing the measured amplitudes by those measured for the intact cells. For some specific individual cells in the population the amplification factor of the integral signal was more than 100 relative to NP scattering. Owing to the heterogeneity of cellular properties, the amplification effect was also heterogeneous. We

found that the higher the NP cluster-related signal, the higher the PTB-related signal. This correlation is in line with physical mechanisms that are involved in PTB generation: the bigger the cluster, the bigger the bubble.

PTBs as optical markers of cell damage—Photothermal bubble-induced damage to individual cells was studied through the visual and PT detection of large PTBs (with a lifetime much longer than 100 ns) in various cells [112]. We also found that 99% of the PTB-positive cells were found to be damaged according to the trypan blue staining test, which indicated the disruption of the cellular membranes. Thus we may conclude that the PTB signal (response or image) indicates cell damage in the case where the PTB lifetime is longer than 100 ns. Thus the PTB can be employed as an optical marker for the real-time detection of the damage at cell level. This property of the PTB may help in optical guidance of the PTB-based therapy. PTBs allow us to obtain several quantitative parameters for a cell population: probability of cell damage at specific fluence, damage threshold fluence, PTB-generation threshold fluence and the degree of cell heterogeneity in the population according to the difference between maximal and minimal damage threshold fluence levels. These data characterize the cells and we have defined the cytometric method for PTB-based analysis of living cells as the laser load test [112,113]. This method can be performed with an optical microscope and also with a flow cytometer providing that the device is equipped with PTB generation and detection units. In our studies, we have shown that the laser load test provides a high sensitivity in monitoring the physiological state of different individual living cells and their systems (hepatocytes and their redox state [114], cell–drug interactions [115], apoptosis of white blood and cancerous cells [116]). Further details on the laser- load test are available in [112,113,117].

PTB therapy

The development of molecularly targeted therapy and gold NPs, which can be optically activated to generate PTBs, suggests that coupling disease-specific molecular (or cellular) targets with NPs for activation of intracellular PTBs could serve as an effective strategy for treatment at the cell level. The NP cluster-bubble mechanism may combine diagnostics, treatment and guidance in one device/process (Figure 17).

- Clusters of NPs can be selectively formed in specific tumor cells for the detection of the disease-specific cells and tissues through NP and PTB optical scattering of low-energy laser pulse (small PTBs);
- Local mechanical destruction of the detected cells/tissues can occur by the generation of intracellular PTBs with diameters above cell damage thresholds;
- Real-time optical guidance of the damage can happen at the cellular level through optical detection of large ‘therapeutic’ PTBs.

Such a combination of three stages in one process and device should significantly improve the efficacy and selectivity of treatment and also does not involve chemotherapy. We defined the described method as laser-activated nano-thermolysis as cell elimination technology (LANTCET).

Cell-level studies of the LANTCET—We have studied the damage to individual K562 cells that were pretreated with 30-nm gold NSPs to pulsed laser irradiation (532 nm, 10 ns) in cell suspension samples *in vitro* (Figure 18). Cell damage probability was analyzed at several different levels of laser fluence: 5, 35 and 90 J/cm^2 for the test and control samples (Figure 18). Cell damage level increased and damage threshold decreased for the cells where NP clusters have been formed during their targeting. Besides the culture cancer cells, we also studied suspensions of the human leukemic and normal stem cells. The samples were obtained from primary patients diagnosed with acute lymphoblast leukemia. There are several

monoclonal antibodies that are considered to be specific for this diagnosis: CD19, CD20 and CD22. We incubated leukemia and normal bone marrow cells *in vitro* with antibodies conjugated to 30-nm gold NSPs. Then the cell samples were exposed to single laser pulses (10 ns, 532 nm) at specific fluence levels. Different antibodies (employed as targeting vectors) yielded different damage levels among leukemia cells (lymphoblasts) after exposure to a single laser pulse at 1.7 J/cm^2, CD19: 84% of the damaged cells; CD20: 33%; and CD22: 67%. Maximal damage level of 100% was achieved at this laser fluence when the combination of the two antibodies – CD19 and CD22 – was used for cell targeting (Figure 18). The level of damage among normal cells that were treated with the same NP–antibody conjugates and laser pulses was found to be within 16%. These cell samples (both normal and tumor) consist of many different types of cells, unlike cultured cells. Despite the heterogeneity of the bone marrow samples, we demonstrated that clustering of NPs, bubble generation and cell damage can be diagnosis-specific. This was demonstrated for a specific diagnosis of acute lymphoblastic leukemia. Additional experimental details can be found in [53,57,89,90,92,94, 95].

PTB method for intracellular delivery—Cell-level therapy assumes the intracellular delivery of the drug or other agent to their ultimate target. This requires a mechanism to surmount the barrier function of the endolysosomal membrane system. One possible mechanism to accomplish endosomal escape can be derived from the basic premise of PTB generation. The disruptive effect of the PTBs can be used at the subcellular level for enhancing intracellular delivery of various diagnostic and therapeutic agents. This method includes several stages (Figure 19).

- The agent to be delivered is linked to the NP, which is also preconjugated with the target-specific vector (such as peptide or monoclonal antibody);
- The NPs are delivered to the cell using two mechanisms: first, the vector–membrane receptor coupling of the NPs at cell membrane, and, second, the internalization of the NPs for intracellular accumulation through receptor-mediated endocytosis [118]. Other mechanisms of internalization, such as pinocytosis and phagocytosis, may also be appropriate modes of entry depending on the cell type examined [119,120];
- PTBs, when being generated inside endosomes, may mechanically rupture the endosomal membrane and thus release the contents of the endosome into the cytoplasm.

Besides the disruption of endosomes, the suggested mechanism may be employed to create temporal small holes in the cellular membrane (poration) to enhance intracellular delivery of the diagnostic and therapeutic agents. The suggested delivery mechanism is principally different from well-known opto- and sono-poration [32,121–125]: the cell outer membrane remains intact; bubbles are generated only in specific endosomes; NPs (or other probes) are secured inside the endosomes; and NP–PTB is an intracellular mechanism that can be applied to individual specific cells. All of these factors will provide improved and safe delivery of the probes to cytosolic targets. In addition, the NP–PTB method can be considered for the delivery of any agents (e.g., drugs and markers) to intracellular targets.

Selective elimination of target tissue—Below we describe two examples of the LANTCET application at microtissue level: recanalization of the occluded arteries and tumor therapy.

Recanalization of occluded and calcified arteries still represents a major challenge when neither a catheter can be guided through a plaque nor can the latter be rapidly lysed with drugs. This causes a significant level of lethal outcomes [126]. Laser-based methods were applied to this problem more than 25 years ago [127–129] and have demonstrated promising results based on

ablation and vaporization of atherosclerotic plaques and thrombi [130–134]. However, long and great efforts did not turn laser angioplasty into a successful clinical tool. This was caused by several principal limitations, such as embolization with large debris, the low and heterogeneous optical absorbance properties of plaque tissues that were used as optical absorbers, restenosis of artery walls and, most importantly, a high risk of thermal damage to an artery wall [135–137]. As a result, the modern laser-based methods were eventually redirected from arteries to veins [135] with their current, rather limited, clinical applications for treating atherosclerotic disease [138]. We have suggested employing NP-generated PTBs for selective mechanical disruption and removal of the plaque or thrombus tissue without thermal and mechanical damage to the arterial wall (Figure 20). PTBs were generated *in vitro* around 250-nm gold NSPs with 10-ns laser pulse at 532 nm. Postmortem plaque samples were treated in the following way: 250-nm gold NPs were horizontally injected into the plaque as a transverse microjet that was directed with a microneedle of 50-μm diameter in the sample plane inside the artery slice (Figure 21). A pulsed laser beam (10 ns, 532 nm, 3.5 J/cm^2) was applied orthogonally and scanned across the surface of the sample to irradiate plaque and arterial wall. The diameter of the laser beam in the sample plane was 20 μm, as was determined with a charge-coupled device camera.

Complete removal of the material was observed after one–ten single laser pulses for plaque tissue (Figure 21B). The size of cleared zones (20–220 μm) was found to be 500–1000-times bigger than the size of the NPs applied. PTB generation did not increase the temperature of the microenvironment outside the PTB and the debris size was below 2 μm. The diameter of the cleared volume (25 μm) was comparable to that of the area of the intersection of the jet (100–150 μm) and the laser beam (20 μm). We observed no generation of the PTB and no optically detectable damage to the wall tissue at equal laser fluence and exposure time. We also evaluated the optical-scattering properties of PTBs for the optical guidance of the process of plaque removal. The optical scattering image in Figure 21D was obtained for the sample shown in Figure 21A during its exposure to the pump laser. PTB-specific signals (bright small white spots in Figure 21D) yielded high amplitude and coincided spatially with the location of the cleared zone, as shown in Figure 21B. The described experiment with human plaque samples demonstrated the potential of the combined action of gold NPs and PTBs for creating a microchannel without damage to the arterial wall.

Photothermal bubble anticancer therapy was studied in an animal model. Rats were implanted with sarcoma cells intra- and subdermally to yield tumors 5–6 mm in diameter that were topically treated with 30 nm gold NSP–IgG conjugates (Figure 22A). A single laser pulse of 532 nm (maximum of light absorbance by NSP), 10-ns duration, 0.75 J/cm^2 fluence, and 3 mm diameter was directed to the central area of the tumor. The fluence level has been chosen to be above the PTB generation threshold for clusters of 30-nm NPs. Control tumors (not treated with NPs) were exposed to identical laser pulses. The viability of the tumors was analyzed in 24 h according to the uptake of Evans Blue dye. Figure 23 shows vertical cross-sections of the two tumor slices: treated with NPs and a single laser pulse (Figure 22C) and treated only with the identical laser pulse (Figure 22D). The NP- and laser-treated tumor showed nonviable (white) area with a diameter close to the laser beam diameter (3–4 mm) and a depth of 1–2 mm, which may indicate diffusion depth of NPs into the tumor. The tumor that underwent laser treatment without pretreatment with NPs showed no signs of any damage and appeared to be viable. The conditions of NP–cell interaction (physiological temperature and 40-min incubation time) were sufficient to provide the formation of NP clusters in tumor cells as previous *in vitro* experiments have shown. Therefore, we may assume that the main mechanism of tumor damage in the animal model is also associated with the cluster–bubble effect.

PTB therapy versus NP & PT therapies

The LANTCET is distinct from NP and laser therapies since it uses another agent – the PTB. The initial therapeutic application of NPs was associated with drug delivery. Those studies focused on methods of drug delivery into cells using NPs as carriers [139]. Usually monoclonal antibodies are used as targeting vectors [139–141]. Development of laser therapy began almost synchronously with the invention of a laser. Laser methods use the photochemical, photomechanical and PT effects of laser interactions with cells and tissues [8,9,17,111,142–152]. Photochemical treatment (known as photodynamic therapy) uses photoactivation of specific chemical agents that become toxic for surrounding cells and tissues when activated by low light power [146–148]. A well-known limitation of photodynamic therapy is that it requires tissue oxygenation for the production of singlet oxygen as a toxic agent, while malignant tissues are usually hypoxic [151]. The idea of using dye contrast agents for photomechanical and PT ablation of target cells has been previously explored, but without successful application to real human tissues [111,144]. Thermal degradation of organic dyes prevents successful completion of dye-based PT procedures. Application of plasmonic NPs as optically activated heat sources [9,10,17,86,109,143,153–156] allowed the enhancement and localization of the effect of hyperthermia; also, NPs have allowed a significant decrease in laser power. However, there are some principal problems that limit selectivity and safety of NP-based PT therapies:

- It is impossible to totally exclude a nonspecific accumulation of NPs in nontarget (normal) cells and tissues that may be thermally damaged while being exposed to laser radiation;
- It is difficult to localize thermal effects within individual target cells, because thermal diffusion during exposure to laser radiation (reported to be from 10^{-4} s to 10^{2} s) expands the laser-induced thermal field over a much larger volume than a single cell, thus damaging collateral cells and tissues.

The main difference of LANTCET from the NP-, laser- and hyperthermia-based methods of diagnostics and therapy is associated with the use of the principally new type of the agent – the PTB. The PTB is not the NP but a physical phenomenon (bubble) that is generated and controlled with a laser pulse around plasmonic NPs at a specific moment and site. The proposed LANTCET technology combines the high specificity of targeting methods (formation of the clusters of NPs only in specific tumor cells), the safety of diagnostics and treatment of tumors with gold NPs, the selectivity of cell damage through PTBs without thermal damage of normal cells and optical guidance of the tumor treatment process through the real-time detection of tumor cells and monitoring of their destruction by registering bubble-specific optical signals. It should be sufficient to form at least one big NP cluster in the target cell to provide damage to that cell through the cluster–bubble mechanism. This would allow minimal concentration of NP conjugates during the administration of NPs. All clinically relevant stages of diagnostics, treatment and treatment monitoring (guidance) can be realized with the help of only one technical microdevice and within several microseconds.

Conclusion

Physical, optical and biomedical properties of the plasmonic NP-generated PT vapor bubbles (NP–PTB) can be summarized as:

- Selective targeting of plasmonic NPs to specific molecules and cells provides the generation of local PTBs at the site of the target;
- Transient nature of the PTB makes it a ‘stealth’ agent that does not exist unless being activated optically on demand;

- Clustering of NPs around the target through the mechanism of receptor-mediated endocytosis and the threshold mechanism of the bubble generation may provide very selective generation of PTBs only around clusters of gold NPs, while no PTBs will be generated around single, nonspecifically coupled NPs. This improves the specificity and selectivity of PTBs over other NP-based agents and probes. This also significantly minimizes the number of NPs required: one cluster of ten to 50 NPs will be sufficient for imaging, diagnosis and therapy;
- The PTB combines optical and mechanical effects for simultaneous diagnosis and therapy at the nano- and microscale;
- The PTBs provide their diagnostic and therapeutic effect through a single event of nano-and micro-second duration, thus eliminating the need for a prolonged treatment and exposure of the sample to laser radiation;
- The biomedical effect of PTBs can be precisely controlled and tuned with fluence of a laser pulse that varies the PTB diameter and life-time: small PTBs can be generated with a low-fluence pulse for noninvasive diagnostic purposes (including imaging), while an increase in the pump laser fluence immediately turns them into disruptive agents that may act at molecular, cellular and tissue levels depending upon the PTB size;
- Being a thermal phenomenon, the PTB at the same time concentrates the heat released by the NP inside the PTB, so for its environment it acts as a ‘cold’ agent, thus preventing thermal damage to tissues and molecules outside the bubble.

These properties allowed us to formulate the concept of PTB theranostics as a process that uses tunable PTBs to detect, treat and guide the target (cell or microtissue) with one agent and one device. PTB theranostics can be realized at molecular, cellular and tissue levels. It employs the safety of the gold NPs (including their approval by FDA), the transient (stealth) nature of on-demand activated PTBs and the ability to tune PTB function from noninvasive imaging to localized damage. Being nonchemical agents, PTBs utilize on the nanoscale the phenomena of light and heat that are natural and essential for all living systems.

Future perspective

The development of theranostic PTB methods and agents will result in a new scientific platform that will generate technologies with superior imaging, diagnostic and therapeutic potential. The combination of the biological safety of gold NPs with the on-demand nature of nanoscale PTBs (that do not physically present in the cell or tissue until being activated) will significantly improve the safety, sensitivity and selectivity of research (molecular imaging, living cell analysis and detection); diagnosis (detection of disease-specific tissue, cells and bacteria with great sensitivity); therapy and surgery (selective elimination of target tissues and cells such as tumors, atherosclerotic plaques, cellular-level hyperthermia and PTB-enhanced drug and probe intracellular delivery by means of the membrane transfection and endosome disruption) and biomedical instruments (e.g., optical microscopy, endoscopy, flow cytometry, laser surgery and angioplasty).

Executive summary

- The mechanism of photothermal bubbles (PTBs) and the target-specific clustering of plasmonic nanoparticles provides selective generation of PTBs with a controllable diameter and lifetime and without thermal impact to the microenvironment outside the PTB.

- PTBs are a new class of highly sensitive and potentially minimally invasive optical probes for cell and molecule detection with a 100–1000-fold improvement on the optical sensitivity relative to that for plasmonic nanoparticles as optical probes.
- The biomedical effect of the PTB can be precisely tuned in individual living cells from noninvasive imaging to localized mechanical, nonthermal damage and elimination of a target by varying the fluence and other parameters of the excitation (pump) laser pulse.
- The mechanisms of PTB generation and detection provide a basis for the integration of diagnosis, therapy and therapy guidance into one theranostic process at cell level that may be supported by one device and can be realized within microseconds.

Acknowledgments

The author appreciates valuable input and support from Ekaterina Lukianova-Hleb from AV Lykov Institute of Heat and Mass Transfer, Jason Hafner, Rebekah Drezek and James McNew (Dr McNew has also kindly provided Figure 19) from Rice University, Jeffrey Myers, Ann Gillenwater and Ehab Hanna from the University of Texas MD Anderson Cancer Center.

Financial & competing interests disclosure

The author acknowledges support from NIH 1R21CA133641 and from the Institute of International Education/SRF (NY, USA). The author has no other relevant affiliations or financial involvement with any organization or entity with a financial interest in or financial conflict with the subject matter or materials discussed in the manuscript apart from those disclosed.

No writing assistance was utilized in the production of this manuscript.

Bibliography

1. Lewinski N, Colvin V, Drezek R. Cytotoxicity of nanoparticles. Small 2008;4(1):26–49. [PubMed: 18165959]
2. Murphy C, Gole A, Stone J, et al. Gold nanoparticles in biology: beyond toxicity to cellular imaging. Acc. Chem. Res 2008;41(12):1721–1730. [PubMed: 18712884]
3. Sokolov K, Follen M, Aaron J, et al. Real-time vital optical imaging of precancer using anti-epidermal growth factor receptor antibodies conjugated to gold nanoparticles. Cancer Res 2003;63(9):1999–2004. [PubMed: 12727808]
4. Javier D, Nitin N, Levy M, Ellington A, Richards-Kortum R. Aptamer-targeted gold nanoparticles as molecular-specific contrast agents for reflectance imaging. Bioconjug. Chem 2008;19(6):1309–1312. [PubMed: 18512972]
5. Nitin N, Javier D, Richards-Kortum R. Oligonucleotide-coated metallic nanoparticles as a flexible platform for molecular imaging agents. Bioconjug. Chem 2007;18(6):2090–2096. [PubMed: 17922545]
6. Maitland K, Gillenwater A, Williams M, El-Naggar A, Descour M, Richards-Kortum R. *In vivo* imaging of oral neoplasia using a miniaturized fiber optic confocal reflectance microscope. Oral Oncol 2008;44(11):1059–1066. [PubMed: 18396445]
7. Yguerabide J, Yguerabide EE. Light-scattering submicroscopic particles as highly fluorescent analogs and their use as tracer labels in clinical and biological applications. II. Experimental characterization. Anal. Biochem 1998;262(2):157–176. [PubMed: 9750129]
8. Pitsillides CM, Joe EK, Wei X, Anderson RR, Lin CP. Selective cell targeting with light absorbing microparticles and nanoparticles. Biophys. J 2003;84(6):4023–4432. [PubMed: 12770906]
9. Loo C, Lowery A, Halas N, West J, Drezek R. Immunotargeted nanoshells for integrated cancer imaging and therapy. Nano Lett 2005;5(4):709–711. [PubMed: 15826113]

10. Tong L, Zhao Y, Huff T, Hansen M, Wei A, Cheng J-X. Gold nanorods mediate tumor cell death by compromising membrane integrity. Adv Mater Deerfield 2007;19(20):3136–3141. [PubMed: 19020672]
11. Liao H, Nehl C, Hafner J. Biomedical applications of plasmon resonant metal nanoparticles. Nanomedicine 2006;1(2):201–208. [PubMed: 17716109]
12. Yao CP, Rahmanzadeh R, Endl E, Zhang ZX, Gerdes J, Hüttman G. Elevation of plasma membrane permeability by laser irradiation of selectively bound nanoparticles. J. Biomed. Opt 2005;10:064012. [PubMed: 16409077]
13. Tam, AC. Overview of photothermal spectroscopy. In: Sell, JA., editor. Photothermal Investigation of Solids and Fluids. MA, USA: Academic Press; 1988. p. 1-34.
14. Boyer D, Tamarat P, Maali A, Lounis B, Orrit M. Photothermal imaging of nanometer-sized metal particles among scatterers. Science 2002;297(5584):1160–1163. [PubMed: 12183624]
15. Hu M, Hartland G. Heat dissipation for Au particles in aqueous solution: relaxation time versus size. J. Phys. Chem. B 2002;106(28):7029–7033.
16. O'Neal DP, Hirsch LR, Halas NJ, Payne JD, West JL. Photo-thermal tumor ablation in mice using near-infrared absorbing nanoparticles. Cancer Lett 2004;209(2):171–176. [PubMed: 15159019]
17. Huang X, El-Sayed IH, Qian W, El-Sayed MA. Cancer cell imaging and photothermal therapy in the near-infrared region by using gold nanorods. J. Am. Chem. Soc 2006;128(6):2115–2120. [PubMed: 16464114]
18. Lin CP, Kelly MW. Cavitation and acoustic emission around laser-heated microparticles. Appl. Phys. Lett 1998;72(22):2800–2802.
19. Lee S, Anderson T, Zhang H, Flotte TJ, Doukas AG. Alteration of cell membrane by stress waves *in vitro*. Ultrasound Med. Biol 1996;22(9):1285–1293. [PubMed: 9123654]
20. Neumann J, Brinkmann R. Nucleation dynamics around single microabsorbers in water heated by nanosecond laser irradiation. J. Appl. Phys 2007;101(11):114701.
21. van Leeuwen TG, Jansen ED, Welch AJ, Borst C. Excimer laser induced bubble: dimensions, theory, and implications for laser angioplasty. Lasers Surg. Med 1996;18(4):381–390. [PubMed: 8732577]
22. Vogel A, Noack J, Hüttmann G, Paltauf G. Mechanisms of femtosecond laser nanosurgery of cells and tissues. Appl. Phys. B 2005;81(8):1015–1047.
23. Hutson S, Ma X. Plasma and cavitation dynamics during pulsed laser microsurgery *in vivo*. Phys. Rev 2007;99(15):158104.
24. Kotaidis V, Dahmen C, von Plessen G, Springer F, Plech A. Excitation of nanoscale vapor bubbles at the surface of gold nanoparticles in water. J. Chem. Phys 2006;124(18):184702. [PubMed: 16709126]
25. Farny H, Wu T, Holt RG, Murray TW, Roy RA. Nucleating cavitation from laser-illuminated nano-particle. Acoust. Res. Lett. Online 2005;6(3):138–143.
26. Vogel A, Linz N, Freidank S, Paltauf G. Femtosecond-laser-induced nanocavitation in water: implications for optical breakdown threshold and cell surgery. Phys. Rev. Lett 2008;100:038102. [PubMed: 18233040]
27. Hüttmann G, Birngruber R. On the possibility of high-precision optothermal microeffects and the measurement of fast thermal denaturation of proteins. IEEE J. Sel. Top. Quantum Electron 1999;5:954–962.
28. Lapotko D. Pulsed photothermal heating of the media during bubble generation around gold nanoparticles. Intern. J. Heat Mass Transf 2009;52(5–6):1540–1543.
29. Hleb E, Lapotko D. Photothermal properties of gold nanoparticles under exposure to high optical energies. Nanotechnology 2008;19(35):355702.
30. Kennedy JE. High-intensity focused ultrasound in the treatment of solid tumours. Nat. Rev. Cancer 2005;5(4):321–327. [PubMed: 15776004]
31. Guzmán H, Nguyen D, Khan S, Prausnitz M. Ultrasound-mediated disruption of cell membranes I: quantification of molecular uptake and cell viability. J. Accoust. Soc. Am 2001;110(1):588–596.
32. Postema M, van Wamel A, Lancee C, de Jong N. Ultrasound-induced encapsulated microbubble phenomena. Ultrasound Med. Biol 2004;30(6):827–840. [PubMed: 15219962]

33. Yavas O, Leiderer P, Park H, et al. Optical reflectance and scattering studies of nucleation and growth of bubbles at a liquid–solid interface induced by pulsed laser heating. Phys. Rev. Lett 1993;70(12): 1830–1833. [PubMed: 10053397]
34. Zohdy M, Tse C, Ye JY, O'Donnell M. Optical and acoustic detection of laser-generated microbubbles in single cells. IEEE Trans. Ultrason. Ferroelectr. Freq. Control 2006;53(1):117–125. [PubMed: 16471438]
35. Marston, PL. Light scattering by bubbles in liquids and its applications to physical acoustics. In: Crim, LA.; Mason, TJ.; Reisse, JL.; Suslick, KS., editors. Sonochemistry and Sonoluminescence. Dordrecht, The Netherlands: Kluwer Academic Publishers; 1999. p. 73-86.
36. Stevenson D, Agate B, Tsampoula X, et al. Femtosecond optical transfection of cells: viability and efficiency. Opt. Express 2006;14(16):7125–7133. [PubMed: 19529083]
37. Prentice P, Cuschieri A, Dholakia K, Prausnitz M, Campbell P. Membrane disruption by optically controlled microbubble cavitation. Nat. Phys 2005;1(2):107–110.
38. Hleb EY, Hu Y, Drezek RA, Hafner JH, Lapotko DO. Photothermal bubbles as optical scattering probes for imaging living cells. Nanomedicine 2008;3(6):797–812. [PubMed: 19025454]
39. Picard FJ, Bergeron MG. Rapid molecular theranostics in infectious diseases. Drug Discov. Today 2000;7(21):1092–1101. [PubMed: 12546841]
40. Hooper JW. The genetic map to theranostics. MLO Med. Lab. Obs 2006;38:22–23. [PubMed: 16838759]
41. Daou TJ, Li L, Reiss P, Josserand V, Texier I. Effect of poly(ethylene glycol) length on the *in vivo* behavior of coated quantum dots. Langmuir 2009;25(5):3040–3044. [PubMed: 19437711]
42. Chanda N, Shukla R, Katti KV, Kannan R. Gastrin releasing protein receptor specific gold nanorods: breast and prostate tumor avid nanovectors for molecular imaging. Nano Lett 2009;9(5):1798–1805. [PubMed: 19351145]
43. Rosi NL, Giljohann DA, Thaxton CS, Lytton-Jean AKR, Han MS, Mirkin CA. Oligonucleotide-modified gold nanoparticles for intracellular gene regulation. Science 2006;312(5776):1027–1030. [PubMed: 16709779]
44. Petrova H, Min H, Hartland G. Photothermal properties of gold nanoparticles. Z. Phys. Chem 2007;221(3):361–376.
45. Hartland G. Measurements of the material properties of metal nanoparticles by time-resolved spectroscopy. Phys. Chem. Chem. Phys 2004;6(23):5263–5274.
46. Link S, El-Sayed MA. Shape and size dependence of radiative, non-radiative and photothermal properties of gold nanocrystals. Int. Rev. Phys. Chem 2000;19(3):409–453.
47. van Leeuwen TG, Jansen ED, Motamedi M, Welch AJ, Borst C. Excimer laser ablation of soft tissue: a study of the content of fast expanding and collapsing bubbles. IEEE J. Quantum Electron 1994;30 (5):1339–1345.
48. Rayleigh L. On the pressure developed in a liquid during the collapse of spherical cavity. Philos. Mag 1917;34:94–98.
49. Brennen, CE. Cavitation and Bubble Dynamics. New York, USA: Oxford University Press; 1995.
50. Ohl CD, Kurz T, Geisler R, Lindau O, Lauterborn W. Bubble dynamics, shock waves and sonoluminescence. Philos. Trans. R. Soc. London Ser. A 1999;357(1751):269–294.
51. Lapotko D, Lukianova-Hleb E, Oraevsky A. Clusterization of nanoparticles during their interaction with living cells. Nanomedicine 2007;2(2):241–253. [PubMed: 17716124]
52. Chan WCW, Chithrani BD. Elucidating the mechanism of cellular uptake and removal of protein-coated gold nanoparticles of different sizes and shapes. Nano Lett 2007;7(6):1542–1550. [PubMed: 17465586]
53. Hleb EY, Hafner JH, Lapotko DO, et al. LANTCET: elimination of solid tumor cells with photothermal bubbles generated around clusters of gold nanoparticles. Nanomedicine 2008;3(5): 647–667. [PubMed: 18817468]
54. Vasiliev L, Hleb E, Shnip A, Lapotko D. Bubble generation in micro-volumes of “nanofluids”. Intern. J. Heat Mass Transf 2009;52(5–6):1534–1539.
55. Lapotko D. Optical excitation and detection of vapor bubbles around plasmonic nanoparticles. Opt. Express 2009;17(4):2538–2556. [PubMed: 19219157]

56. Lukianova-Hleb E, Lapotko D. Influence of transient environmental photothermal effects on optical scattering by gold nanoparticles. Nano Lett 2009;9(5):2160–2166. [PubMed: 19374436]
57. Lapotko D, Lukianova E, Shnip A, et al. Laser activated nanothermolysis of leukemia cells monitored by photothermal microscopy. Proc. SPIE 2005;5697:82–89.
58. Lapotko D, Lukianova E, Chizhik S. Methods for monitoring and imaging nanoparticles in cells. Proc. SPIE 2007;6447:644703.
59. Bartels DM, Crowell RA. Laser-initiated chemical reactions in carbon suspensions. J. Phys. Chem. A 2002;106(43):10072–10078.
60. Lukianova-Hleb E, Mrochek A, Lapotko D. Method for disruption and re-canalization of atherosclerotic plaques in coronary vessels with photothermal bubbles generated around gold nanoparticles. Lasers Surg. Med 2009;41(3):240–247. [PubMed: 19291755]
61. Neumann J, Brinkmann R. Boiling nucleation on melanosomes and microbeads transiently heated by nanosecond and microsecond laser pulses. J. Biomed. Opt 2005;10(2):024001. [PubMed: 15910075]
62. Anderson RR, Parrish JA. Selective photothermolysis: precise microsurgery by selective absorption of pulsed radiation. Science 1983;220(4596):524–527. [PubMed: 6836297]
63. Gersman S. Theoretical modeling of laser induced explosive pressure generation and vaporization in pigmented cells. Proc. SPIE 2000;3902:41–52.
64. Juhasz T, Kastis GA, Suarez C, Bor Z, Bron WE. Time-resolved observations of shock waves and cavitation bubbles generated by femtosecond laser pulses in corneal tissue and water. Lasers Surg. Med 1996;19(1):23–31. [PubMed: 8836993]
65. Roegener J, Lin CP. Photomechanical effects: experimental studies of pigment granule absorption, cavitation, and cell damage. Proc. SPIE 2000;3902:35–40.
66. Lin CP, Kelly MW, Sibayan SAB, Latina MA, Anderson RR. Selective cell killing by microparticle absorption of pulsed laser radiation. IEEE J. Sel. Top. Quantum Electron 1999;5:963–968.
67. Schaffer B, Nishimura N, Glezer EN, Kim AMT, Mazur E. Dynamics of femtosecond laser-induced breakdown in water from femtoseconds to microseconds. Opt. Express 2002;10(3):196–203. [PubMed: 19424350]
68. Francois L, Mostafavi M, Belloni J, Delouis J-F, Delaire J, Feneyrou P. Optical limitation induced by gold clusters. J. Phys. Chem. B 2000;104(26):6133–6137. 1. Size effect.
69. Volkov AN, Sevilla C, Zhigilei LV. Numerical modeling of short pulse laser interaction with Au nanoparticle surrounded by water. Appl. Surf. Sci 2007;253(15):6394–6399.
70. Kotaidis V, Plech A. Cavitation dynamics on the nanoscale. Appl. Phys. Lett 2005;87:213102.
71. Krasovitski B, Kislev H, Kimmel E. Modeling photothermal and acoustical induced microbubble generation and growth. Ultrasonics 2007 1–4;47:90–101. [PubMed: 17910969]
72. Otter M. Temperature dependance of the optical constants of heavy metals. Z. Phys 1961;161:539–549.
73. Hu M, Petrova H, Hartland GV. Investigation of the properties of gold nanoparticles in aqueous solution at extremely high lattice temperatures. Chem. Phys. Lett 2004;391(4–6):220–225.
74. Plech A, Cerna R, Kotaidis V, Hudert F, Bartels A, Dekorsy T. A surface phase transition of supported gold nanoparticles. Nano Lett 2007;7(4):1026–1031. [PubMed: 17352505]
75. Inasawa S, Sugiyama M, Yamaguchi Y. Laser-induced shape transformation of gold nanoparticles below the melting point: the effect of surface melting. J. Phys. Chem. B 2005;109(8):3104–3111. [PubMed: 16851329]
76. Inasawa S, Sugiyama M, Noda S, Yamaguchi Y. Spectroscopic study of laser-induced phase transition of gold nanoparticles on nanosecond time scales and longer. J. Phys. Chem. B 2006;110(7):3114–3119. [PubMed: 16494317]
77. Dayton PA, Chomas JE, Lunn AFH, et al. Optical and acoustical dynamics of microbubble contrast agents inside neutrophils. Biophys. J 2001;80(3):1547–1556. [PubMed: 11222315]
78. Francois L, Mostafavi M, Belloni J, Delaire J. Optical limitation induced by gold clusters: mechanism and efficiency. Phys. Chem. Chem. Phys 2001;3(22):4965–4971.
79. Lapotko D, Lukianova K, Shnip A. Photothermal responses of individual cells. J. Biomed. Opt 2005;10(1):014006.

80. Lapotko D, Lukianova K. Laser-induced micro-bubbles in cells. Int. J. Heat Mass Trans 2005;48(1): 227–234.
81. Chan WCW, Chithrani BD, Ghazani AA. Determining the size and shape dependence of gold nanoparticle uptake into mammalian cells. Nano Lett 2006;6(4):662–668. [PubMed: 16608261]
82. Shukla R, Bansal V, Chaudhary M, Basu A, Bhonde RR, Sastry M. Biocompatibility of gold nanoparticles and their endocytotic fate inside the cellular compartment: a microscopic overview. Langmuir 2005;21(23):10644–10654. [PubMed: 16262332]
83. Oberdorster G, Oberdorster E, Oberdorster J. Nanotoxicology: an emerging discipline evolving from studies of ultrafine particles. Environ. Health Perspect 2005;113(7):823–839. [PubMed: 16002369]
84. Connor E, Mwamuka J, Gole A, Murphy C, Wyatt M. Gold nanoparticles are taken up by human cells but do not cause acute cytotoxicity. Small 2005;1(3):325–327. [PubMed: 17193451]
85. Huff T, Hansen M, Zhao Y, Cheng J-X, Wei A. Controlling the cellular uptake of gold nanorods. Langmuir 2007;23(4):1596–1599. [PubMed: 17279633]
86. Takahashi H, Niidome Y, Niidome T, Kaneko K, Kawasaki H, Yamada H. Modification of gold nanorods using phosphatidylcholine to reduce cytotoxicity. Langmuir 2006;22(1):2–5. [PubMed: 16378388]
87. Cortesi R, Esposito E, Menegatti E, Gambari R, Nastruzzi C. Effect of cationic liposome composition on *in vitro* cytotoxicity and protective effect on carried DNA. Int. J. Pharm 1996;139(1–2):69–78.
88. Mirska D, Schirmer K, Funari S, Langner A, Dobner B, Brezesinski G. Biophysical and biochemical properties of a binary lipid mixture for DNA transfection. Colloids Surf. B 2005;40(1):51–59.
89. Lapotko D, Lukianova-Hleb E, Oraevsky A, et al. Photothermal and photoacoustic processes in laser activated nano-thermolysis of cells. Proc. SPIE 2007;6437:64370C.
90. Lapotko D, Lukianova E, Oraevsky A. Selective laser nano-thermolysis of human leukemia cells with microbubbles generated around clusters of gold nanoparticles. Lasers Surg. Med 2006;38(6):631–642. [PubMed: 16736503]
91. Conjusteau A, Ermilov S, Lapotko D, et al. Metallic nanoparticles as optoacoustic contrast agents for medical imaging. Proc. SPIE 2006;6086:60860K.
92. Lapotko D, Lukianova E, Potapnev M, Aleinikova O, Oraevsky A. Method of laser activated nanothermolysis for elimination of tumor cells. Cancer Lett 2006;239(1):36–45. [PubMed: 16202512]
93. Lapotko D. Laser-induced bubbles in living cells. Lasers Surg. Med 2006;38(3):240–248. [PubMed: 16470847]
94. Lapotko D, Lukianova-Hleb E, Hafner J, et al. LANTCET: laser nanotechnology for screening and treatment tumor *ex vivo* and *in vivo*. Proc. SPIE 2007;6735:673516.
95. Lapotko D, Lukianova-Hleb E, Hafner J. Nanocluster-bubble photothermal nanotechnology for anti-cancer applications. Proc. SPIE 2007;6734:67340E.
96. Rost, FWD. Quantitative Fluorescence Microscopy. Cambridge, UK: Cambridge University Press; 1991. Applications of microfluorometry; p. 250
97. Lapotko D. Laser photothermal microscopy for functional imaging of live cells. Microsc. Anal 2002;3:123–126.
98. Lapotko D, Romanovskaya T, Shnip A, Zharov V. Photothermal time-resolved imaging of living cells. Lasers Surg. Med 2002;31(1):53–63. [PubMed: 12124716]
99. Baumgart J, Bintig W, Ngezahayo A, Ertmer W, Lubatschowski H, Heisterkamp A. Live cell opto-injection by femtosecond laser pulses. Proc. SPIE 2007;6435:643512.
100. Coussios C, Farny C, Haar G, Roy R. Role of acoustic cavitation in the delivery and monitoring of cancer treatment by high-intensity focused ultrasound (HIFU). Int. J. Hyperthermia 2007;23(2): 105–120. [PubMed: 17578336]
101. Liu HL, Chen WS, Chen JS, Shih TC, Chen YY, Lin WL. Cavitation-enhanced ultrasound thermal therapy by combined low- and high-frequency ultrasound exposure. Ultrasound Med. Biol 2006;32 (5):759–767. [PubMed: 16677935]
102. McDannold N, Vykhodtseva N, Hynynen K. Microbubble contrast agent with focused ultrasound to create brain lesions at low power levels: MR imaging and histologic study in rabbits. Radiology 2006;241(1):95–106. [PubMed: 16990673]

103. Guzmán H, Nguyen D, Khan S, Prausnitz M. Ultrasound-mediated disruption of cell membranes. I. Quantification of molecular uptake and cell viability. J. Accoust. Soc. Am 2001;110(1):597–606.
104. Schlicher RK, Radhakrishna H, Tolentino TP, Apkarian RP, Zarnitsyn V, Prausnitz MR. Mechanism of intracellular delivery by acoustic cavitation. Ultrasound Med. Biol 2006;32(6):915–924. [PubMed: 16785013]
105. Ohl CD, Wolfrum B. Detachment and sonoporation of adherent HeLa cells by shock wave-induced cavitation. Biochim. Biophys. Acta 2003;1624(1–3):131–138. [PubMed: 14642823]
106. van Wamel A, Bouakaz A, Versluis M, de Jong N. Micromanipulation of endothelial cells: ultrasound–microbubble–cell interaction. Ultrasound Med. Biol 2004;30(9):1255–1258. [PubMed: 15550330]
107. Huang X, Jain P, El-Sayed I, El-Sayed M. Gold nanoparticles: interesting optical properties and recent applications in cancer diagnostics and therapy. Nanomedicine 2007;2(5):681–693. [PubMed: 17976030]
108. Pissuwan D, Valenzuela SM, Cortie MB. Therapeutic possibilities of plasmonically heated gold nanoparticles. Trends Biotechnol 2006;24(2):62–67. [PubMed: 16380179]
109. Gobin A, Lee MH, Halas N, James W, Drezek R, West J. Near-infrared resonant nanoshells for combined optical imaging and photothermal cancer therapy. Nano Lett 2007;7(7):1929–1934. [PubMed: 17550297]
110. Lowery R, Gobin AM, Day ES, Halas NJ, West JL. Immunonanoshells for targeted photothermal ablation of tumor cells. Int. J. Nanomedicine 2006;1(2):149–154. [PubMed: 17722530]
111. Camerin M, Rello S, Villanueva A, et al. Photothermal sensitisation as a novel therapeutic approach for tumours: studies at the cellular and animal level. Eur. J. Cancer 2005;41:1203–1212. [PubMed: 15911245]
112. Lapotko D, Shnip A, Lukianova E. Photothermal detection of laser-induced damage in single intact cells. Lasers Surg. Med 2003;33(5):320–329. [PubMed: 14677159]
113. Lapotko D, Lukianova E. Influence of physiological conditions on laser damage thresholds for blood, heart, and liver cells. Lasers Surg. Med 2005;36(1):13–21. [PubMed: 15662628]
114. Lapotko D, Romanovskaya T, Gordiyko E. Photothermal monitoring of redox state of respiratory chain in single live cells. Photochem. Photobiol 2002;75(5):519–526. [PubMed: 12017479]
115. Lapotko D, Romanovskaya T, Zharov V. Photothermal images of live cells in presence of drug. J. Biomed. Opt 2002;7(3):425–434. [PubMed: 12175293]
116. Lapotko D. Monitoring of apoptosis in intact single cells with photothermal microscope. Cytometry 2004;58A:111–119. [PubMed: 15057964]
117. Lapotko D, Zharov V. Spectral evaluation of laser-induced cell damage with photothermal microscopy. Lasers Surg. Med 2005;36(1):22–30. [PubMed: 15662629]
118. Wiley H, Burke P. Regulation of receptor tyrosine kinase signaling by endocytic trafficking. Traffic 2001;2(1):12–18. [PubMed: 11208164]
119. Wiley H. Trafficking of the ErbB receptors and its influence on signaling. Exp. Cell Res 2003;284 (1):78–88. [PubMed: 12648467]
120. Ceresa B, Schmid S. Regulation of signal transduction by endocytosis. Curr. Opin. Cell Biol 2000;12 (2):204–210. [PubMed: 10712919]
121. Rapoport N, Gao Z, Kennedy A. Multifunctional nanoparticles for combining ultrasonic tumor imaging and targeted chemotherapy. J. Natl Cancer Inst 2007;99(14):1095–1106. [PubMed: 17623798]
122. Iwanaga K, Tominaga K, Yamamoto K, et al. Local delivery system of cytotoxic agents to tumors by focused sonoporation. Cancer Gene Ther 2007;14(1):354–363. [PubMed: 17273182]
123. Korpanty G, Carbon J, Grayburn P, Fleming J, Brekken R. Monitoring response to anticancer therapy by targeting microbubbles to tumor vasculature. Clin. Cancer Res 2007;13(1):323–330. [PubMed: 17200371]
124. Gerstman B, Thompson C, Jacques S, Rogers M. Laser induced bubble formation in the retina. Lasers Surg. Med 1996;18(1):10–21. [PubMed: 8850461]

125. Jacques S, McAuliffe D. The melanosome: threshold temperature for explosive vaporization and internal absorption coefficient during pulsed laser irradiation. Photochem. Photobiol 1991;53(6): 769–775. [PubMed: 1886936]
126. Valenti R, Migliorini A, Signorini U, et al. Impact of complete revascularization with percutaneous coronary intervention on survival in patients with at least one chronic total occlusion. Eur. Heart J 2008;29(19):2336–2342. [PubMed: 18682446]
127. Lee C, Ikeda R, Kozina J, Mason D. Laser dissolution of coronary atherosclerotic obstruction. Am. Heart J 1981;102(6):1074–1075. [PubMed: 7315706]
128. Abela C, Normann S, Cohen D, Feldman R, Geiser E, Conti C. Effects of carbon dioxide, Nd–AG, and argon laser radiation on coronary atheromatous plaques. Am. J. Cardiol 1982;50(6):1199–1205. [PubMed: 6816057]
129. Choy D, Stertzer S, Rotterdam H, Bruno M. Laser coronary angioplasty: experience with 9 cadaver hearts. Am. J. Cardiol 1982;50(6):1209–1211. [PubMed: 6216806]
130. Borst C. Percutaneous recanalization of arteries: status and prospects of laser angioplasty with modified fibre tips. Lasers Med. Sci 1987;2(3):137–151.
131. Benett W, Broughton K, Celliers P, et al. 2002 US6368318.
132. Ginsburg, R.; Geschwind, H. Laser Angioplasty. 2nd edition. Mount Kisco, NY, USA: Futura Publishing Inc.; 1992. p. 205-215.
133. Deckelbaum L. Cardiovascular applications of laser technology. Lasers Surg. Med 1994;15(4):315–341. [PubMed: 7885167]
134. White R, White G, Vlasak J, Fujitani R, Kopchok G. Histopathology of human laser thermal angioplasty recanalization. Lasers Surg. Med 1988;8(5):469–476. [PubMed: 2976445]
135. Kalra M, Gloviczki P. Fifteen years ago laser was supposed to open arteries, now it is supposed to close veins: what is the reality behind the tool? Perspect. Vasc. Surg. Endovasc. Ther 2006;18(1): 3–8. [PubMed: 16628315]
136. Lammer J. Laser angioplasty of peripheral arteries: an epilogue? Cardiovasc. Intervent. Radiol 1995;18(1):1–8. [PubMed: 7788626]
137. Isner J, Donaldson R, Funai J, et al. Factors contributing to perforations resulting from laser coronary angioplasty: observations in an intact human postmortem preparation of intraoperative laser coronary angioplasty. Coronary Artery Surg 1985;72(3 Pt 2):II191–II199.
138. Shafique S, Nachreiner R, Murphy M, Cikrit D, Sawchuk A, Dalsing M. Recanalization of infrainguinal vessels: silverhawk, laser, and the remote superficial femoral artery endarterectomy. Semin. Vasc. Surg 2007;20(1):29–36. [PubMed: 17386361]
139. de Lima M, Shpall E. *Ex-vivo* purging of hematopoietic progenitor cells. Curr. Hematol. Rep 2004;3 (4):257–264. [PubMed: 15217555]
140. Alvarnas J, Forman S. Graft purging in autologous bone marrow transplantation: a promise not quite fulfilled. Oncology 2004;18(7):867–876. [PubMed: 15255171]
141. Gribben, J. Hematopoietic Cell Transplantation. 2nd edition. Thomas, E.; Blume, K.; Forman, S., editors. Malden, MA, USA: Blackwell Science; 1999.
142. Wang F, Jay D. Chromophore-assisted laser inactivation (CALI): probing protein function *in situ* with a high degree of spatial and temporal resolution. Trends Cell. Biol 1996;6(11):442–445. [PubMed: 15157516]
143. Huff T, Tong L, Zhao Y, Hansen M, Cheng Ji-Xin, Wei A. Hyperthermic effects of gold nanorods on tumor cells. Nanomedicine 2007;2(1):125–132. [PubMed: 17716198]
144. Jay D. Selective destruction of protein function by chromophore-assisted laser inactivation. Proc. Natl Acad. Sci. USA 1988;85(15):5454–5458. [PubMed: 3399501]
145. Zic J. The treatment of cutaneous T-cell lymphoma with photopheresis. Dermatol. Ther 2003;16(4): 337–346. [PubMed: 14686977]
146. Hasan, T.; Ortel, B.; Moor, A.; Pogue, B. Holland–Frei Cancer Medicine. 6th Edition. Ontario, Canada: BC Decker, Inc.; 2003. Cancer Medicine; p. 605-622.
147. Dougherty TJ, Gomer CJ, Henderson BW, et al. Photodynamic therapy. J. Natl Cancer Inst 1998;90 (12):889–905. [PubMed: 9637138]

148. Wilson B. Photodynamic therapy for cancer: principles. Can. J. Gastroenterol 2002;16(6):393–396. [PubMed: 12096303]

149. Chen X, Drain C. Photodynamic therapy using carbohydrate conjugated porphyrins. Drug Design Reviews 2004;1(3):215–234.

150. El-Sayed I, Huang X, El-Sayed M. Surface plasmon resonance scattering and absorption of anti-EGFR antibody conjugated gold nanoparticles in cancer diagnostics: applications in oral cancer. Nano Lett 2005;5(5):829–834. [PubMed: 15884879]

151. Zeng Q, Baker I, Loudis J, Liao Y, Hoopes P. Synthesis and heating effect of iron/iron oxide composite and iron oxide nanoparticles. Proc. SPIE 2007;6440:64400H.

152. Dinauer N, Balthasar S, Weber C, Kreuter J, Langer K, von Briesen H. Selective targeting of antibody-conjugated nanoparticles to leukemic cells and primary T-lymphocytes. Biomaterials 2005;26(29):5898–5906. [PubMed: 15949555]

153. Kam N, O'Connell M, Wisdom J, Dai H. Carbon nanotubes as multifunctional biological transporters and near-infrared agents for selective cancer cell destruction. Proc. Natl Acad. Sci. USA 2005;102 (33):11600–11605. [PubMed: 16087878]

154. Seol Y, Carpenter A, Perkins T. Gold nanoparticles: enhanced optical trapping and sensitivity coupled with significant heating. Opt. Lett 2006;31(16):2429–2431. [PubMed: 16880845]

155. Shen N, Datta B, Schaffer C, LeDuc P, Ingber D, Mazur E. Ablation of cytoskeletal filaments and mitochondria in live cells using a femtosecond laser nanoscissor. Mech. Chem. Biosystems 2005;2 (1):17–25.

156. Koenig K, Krauss O, Riemann I. Intratissue surgery with 80 MHz nanojoule femtosecond laser pulses in the near infrared. Opt. Express 2002;10(3):171–176. [PubMed: 19424346]

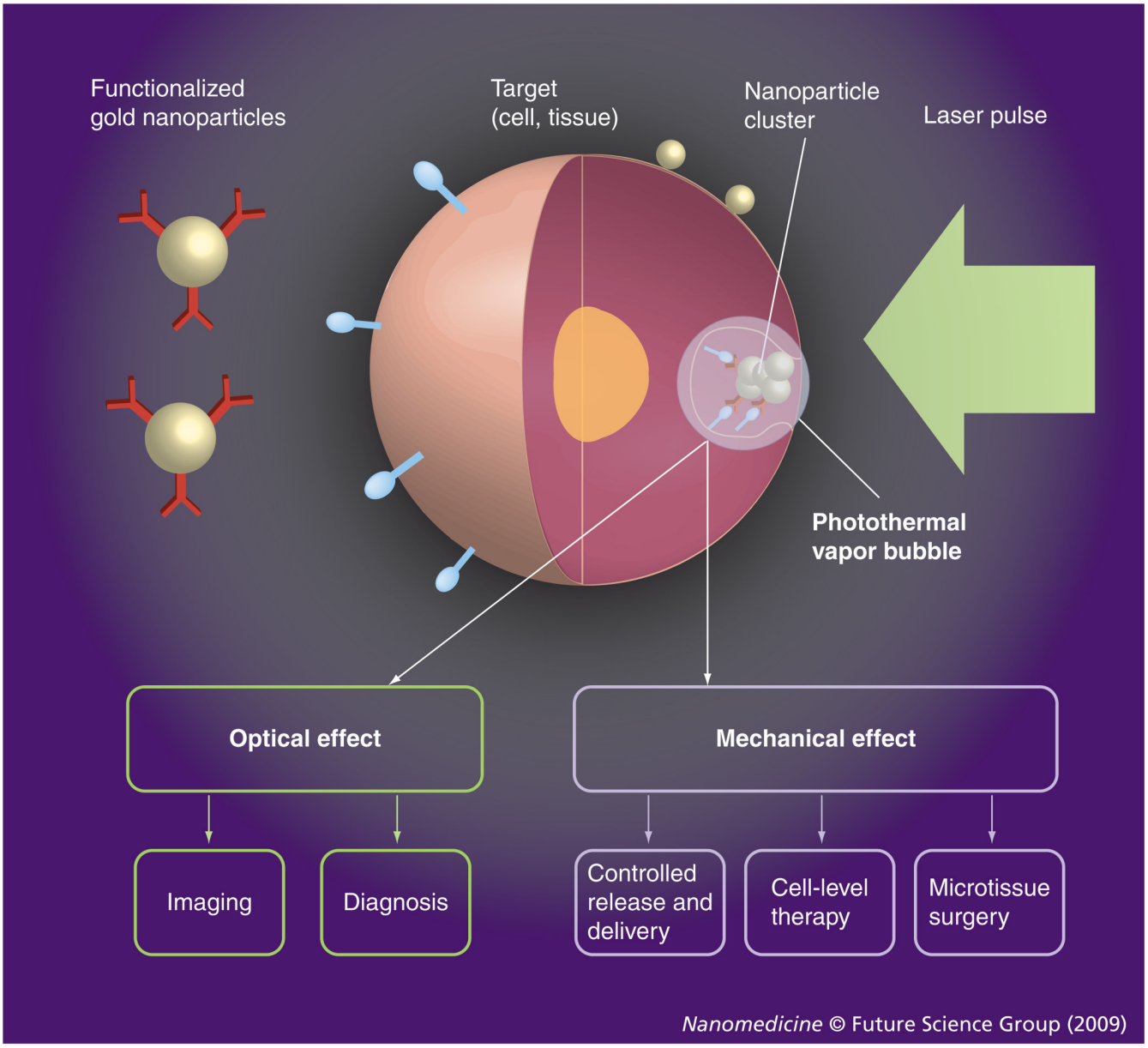

Figure 1. Functionalized gold nanoparticles form a cluster around a target molecule and when excited with a short laser pulse act as a heat source, thus generating an intracellular photothermal vapor bubble

Optical and mechanical effects of the bubble can be controlled through the laser parameters to tune the bubble to diagnostic or therapeutic task.

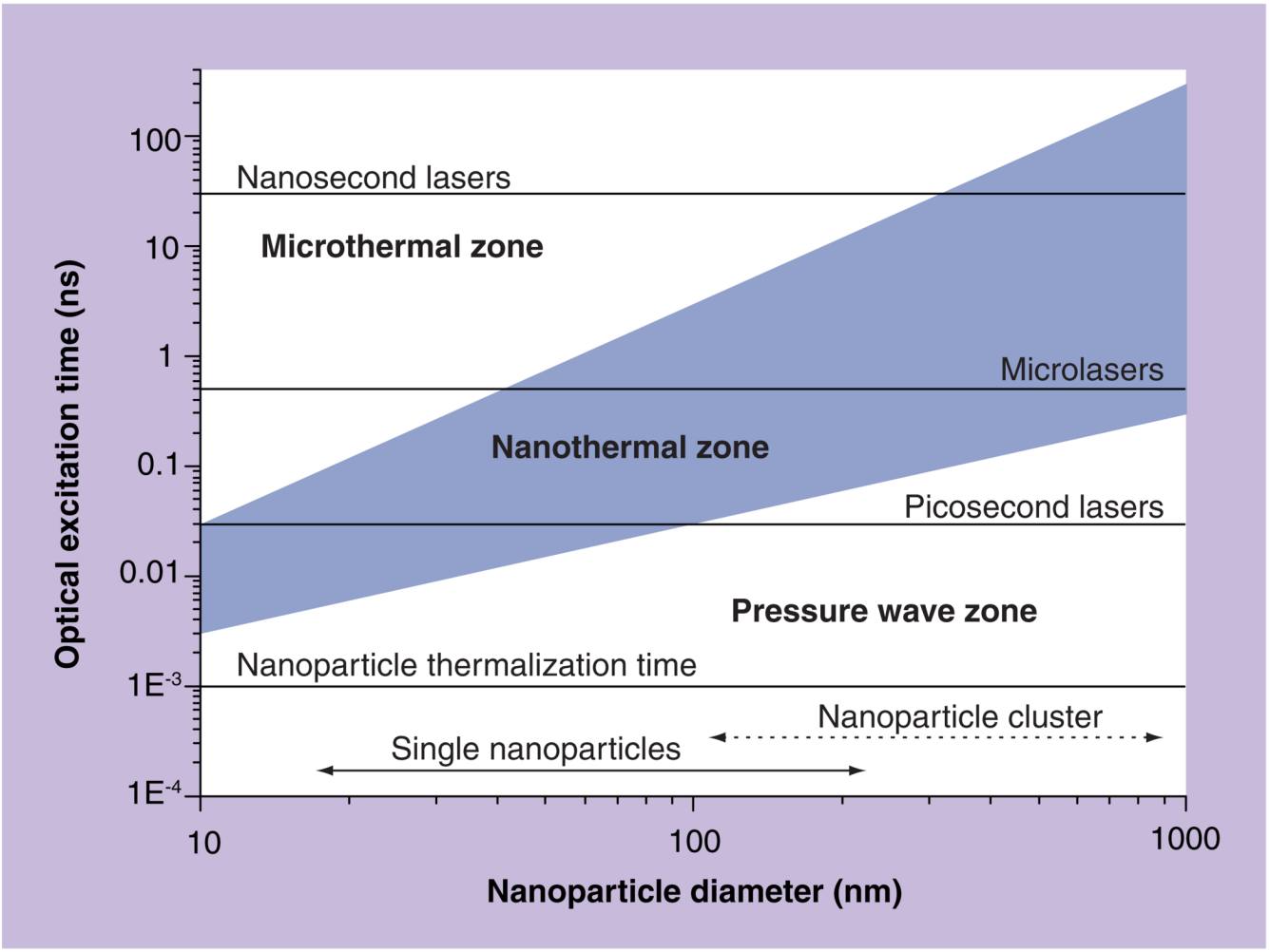

Figure 2. Photothermal processes generated by plasmonic nanoparticles due to optical absorption of a laser pulse and follow up thermalization of the nanoparticle

Bubble mode is shown in blue.

Reproduced with permission from [55].

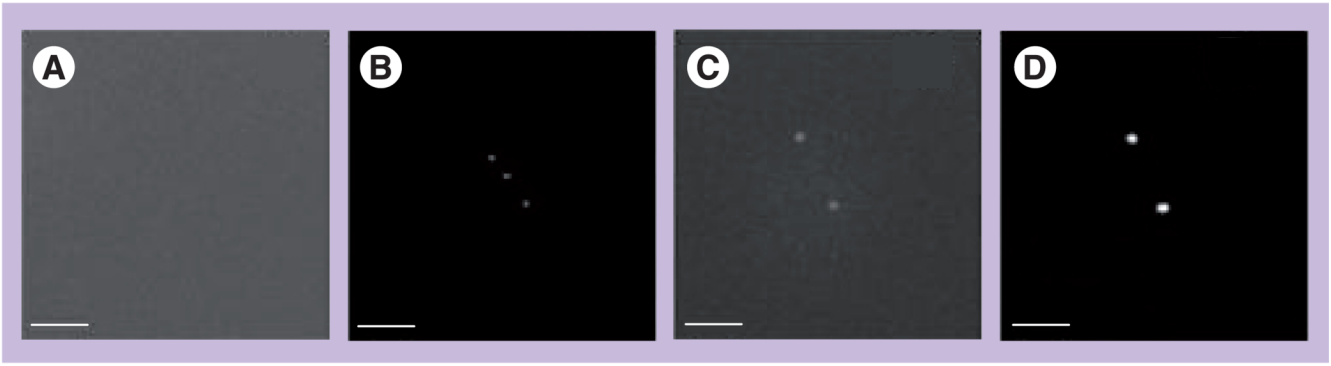

Figure 3. Time-resolved optical scattering images

Obtained for **(A)** 30 nm gold nanoparticles (NPs; no pulse), **(B)** 30-nm gold NPs exposed to a single pump laser pulse (532 nm, 0.5 ns, 0.9 J/cm^2), **(C)** clusters of 30-nm gold NPs (no pulse), **(D)** clusters of 30-nm gold NPs exposed to a single pump laser pulse (532 nm,0.5 ns, 0.12 J/cm^2). The images **(B & D)** were obtained with a 9-ns time delay relative to the pump pulse; scale bar is equal to 6 μm.

Reproduced with permission from [55].

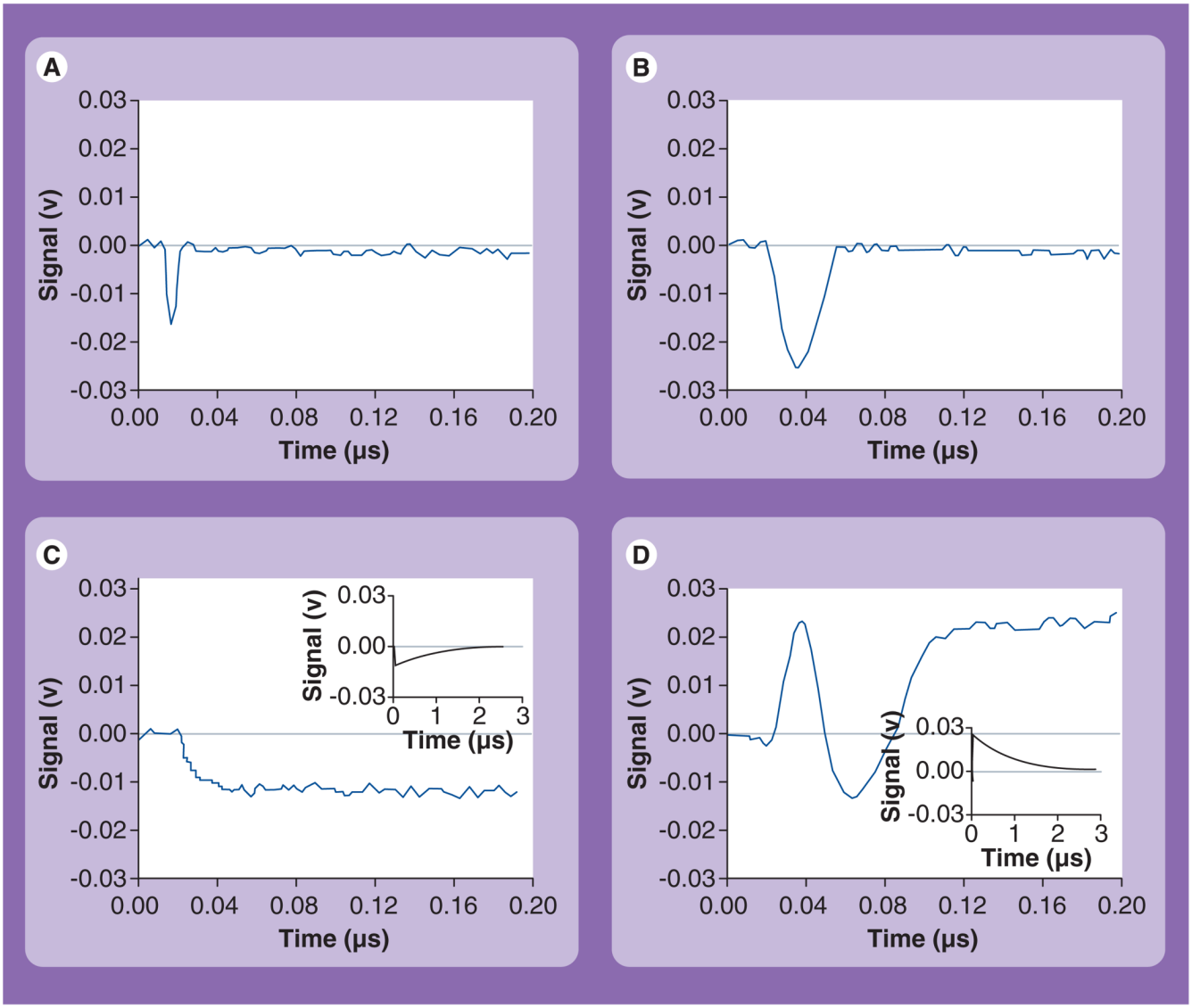

Figure 4. Time responses (demonstrating the decrease of the probe laser intensity owing to the integral scattering effect) obtained from various objects exposed to a single pump pulse (532 nm, 0.5 ns)

(A) Photothermal bubbles (PTBs) around 30-nm gold nanoparticles (NPs) (0.9 J/cm^2), **(B)** PTBs around the cluster of 30-nm gold NPs (0.9 J/cm^2), **(C)** thermal signal in the sample of 30-nm gold NPs at a fluence below the PTB threshold (0.5 J/cm^2), **(D)** superimposed signal os the PTB and thermal field in the sample with hemoglobin as homogenous absorber; the inserts in **(C & D)** show relaxation of bulk thermal signals at full time scales.
Reproduced with permission from [55].

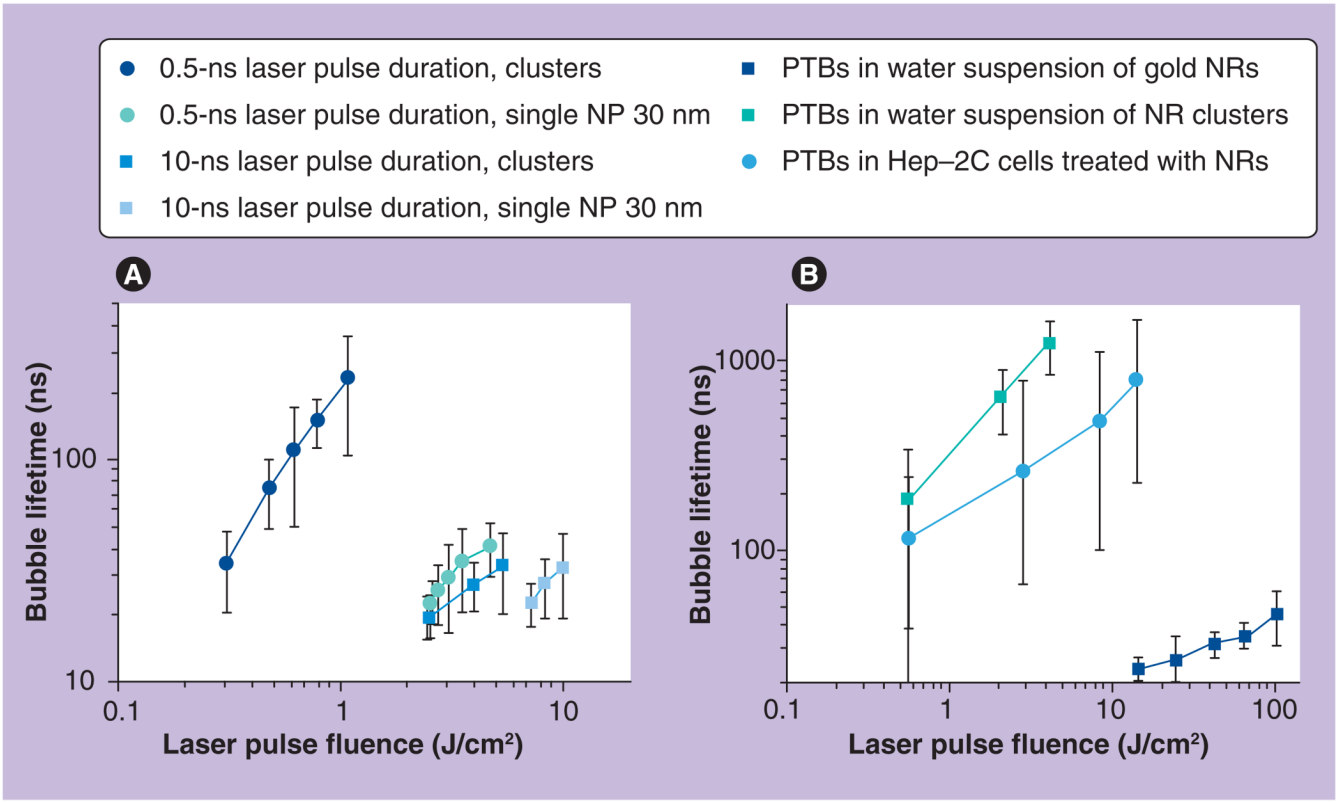

Figure 5. Photothermal bubble lifetimes versus fluence, duration and wavelength of the pump laser pulse

(A) NPs and their clusters in water exposed to the pump pulse with the wavelength 532 nm and duration 0.5 and 10 ns. **(B)** NRs and their clusters in water and in living cells exposed to the pump pulse with the wavelength 750 nm and duration 10 ns.
NP: Nanoparticle; NR: Nanorod; PTB: Photothermal bubble.
Reproduced with permission from [53].

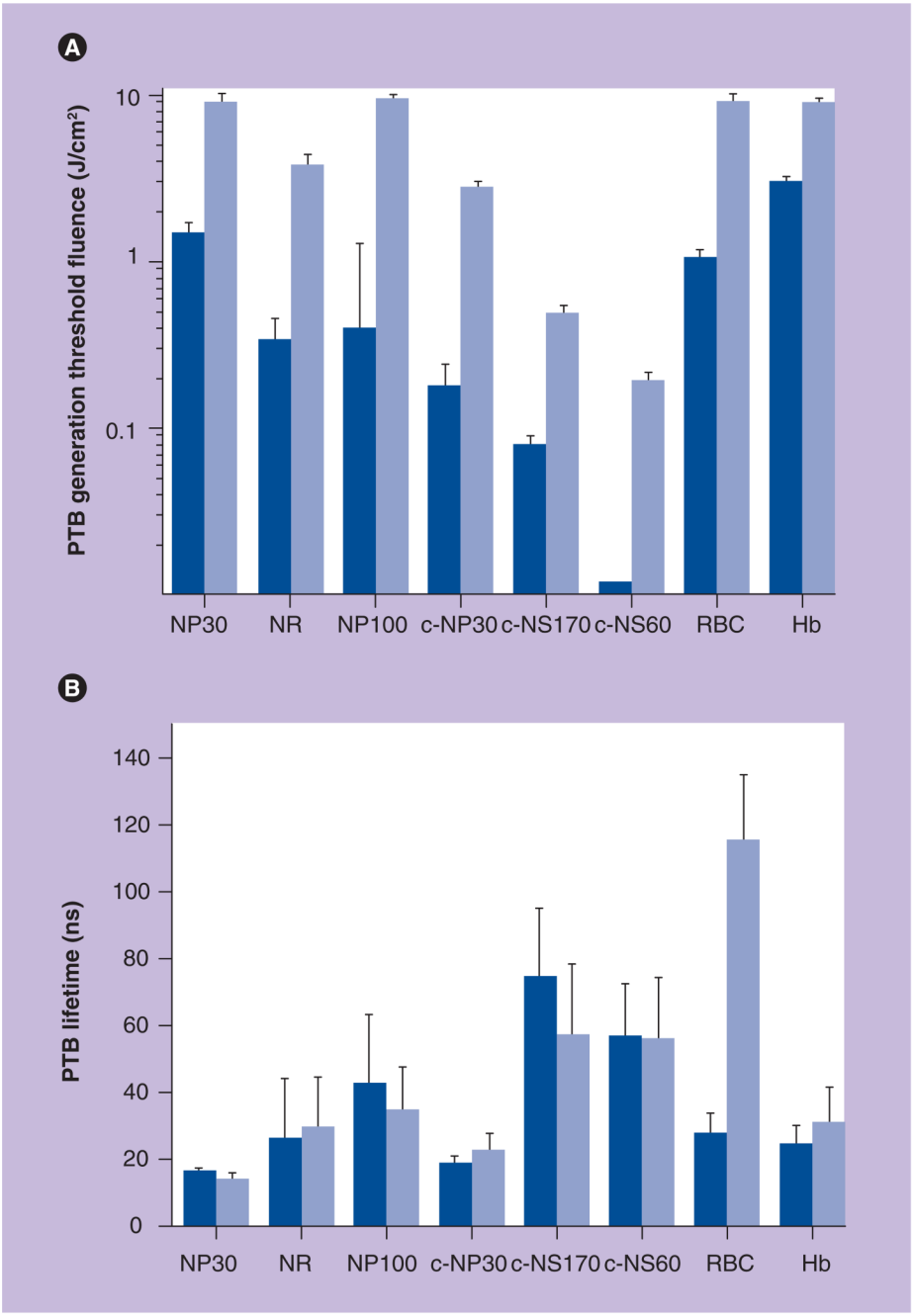

Figure 6. Influence of nanoparticle size, aggregation state and duration of pump laser pulse on the photothermal bubble generation threshold fluence

Photothermal bubble generation threshold fluence **(A)** and lifetime at the threshold fluence **(B)** for NP30, gold NRs, NP100, cNP30, cNS170, cNS60 and for micro- and macro-absorbers: RBCs and Hb. Dark blue columns: 0.5-ns pulse; light blue columns: 10-ns pulse at 532 nm. cNP30: Clusters of 30-nm nanospheres; cNS60: 60-nm gold nanshells; cNS170: 170-nm gold nanoshells; Hb: Homogeneous hemoglobin solution; NP30: Single 30-nm gold nanospheres; NP100: 100-nm gold nanospheres; NR: Nanorod; PTB: Photothermal bubble; RBC: Red blood cell.
Reproduced with permission from [55].

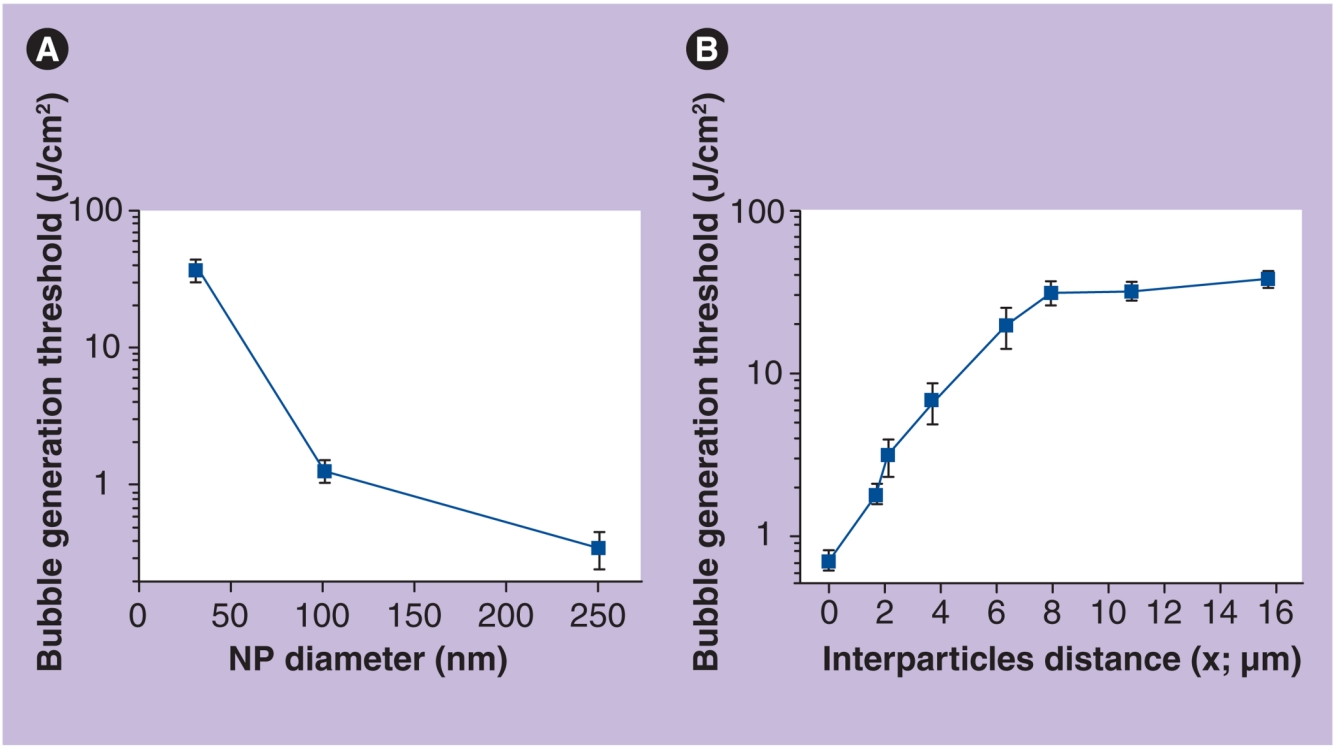

Figure 7. Bubble generation threshold as a function of (A) nanoparticle diameter and concentration (B)

Thresholds of laser-induced bubble generation around 30-nm spherical single NPs as a function of the concentration is presented through the influence of interparticle distance; the laser pulse is 10 ns at 532 nm.

NP: Nanoparticle.

Reproduced with permission from [55].

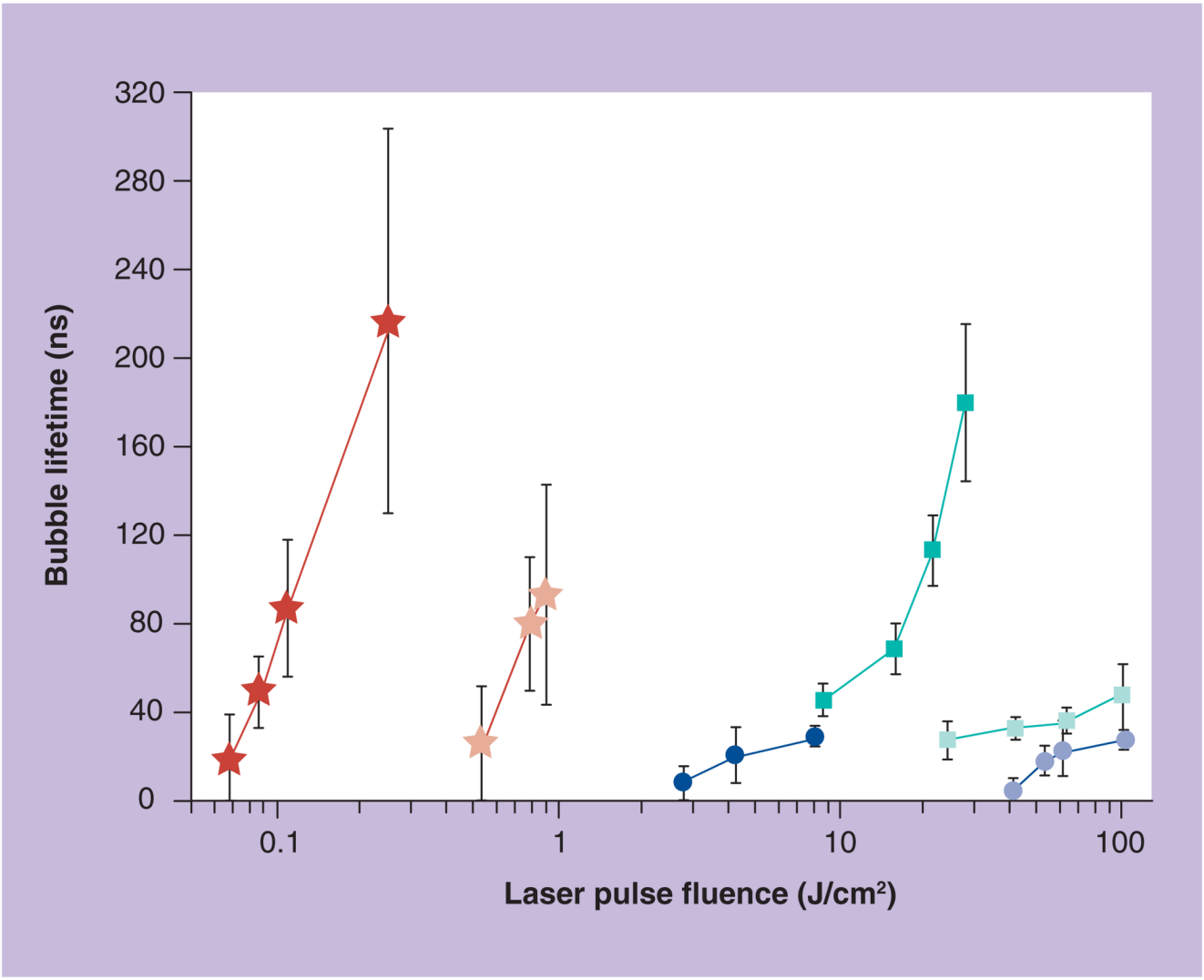

Figure 8. Lifetime of the photothermal bubbles generated around gold nanoparticles versus fluence of the single 10-ns laser pulse with a wavelength of 750 nm (hollow circle: spheres; hollow square: rods; hollow asterisk: shells) and 532 nm (solid circle: spheres; solid square: rods; solid asterisk: shells)

Reproduced with permission from [29].

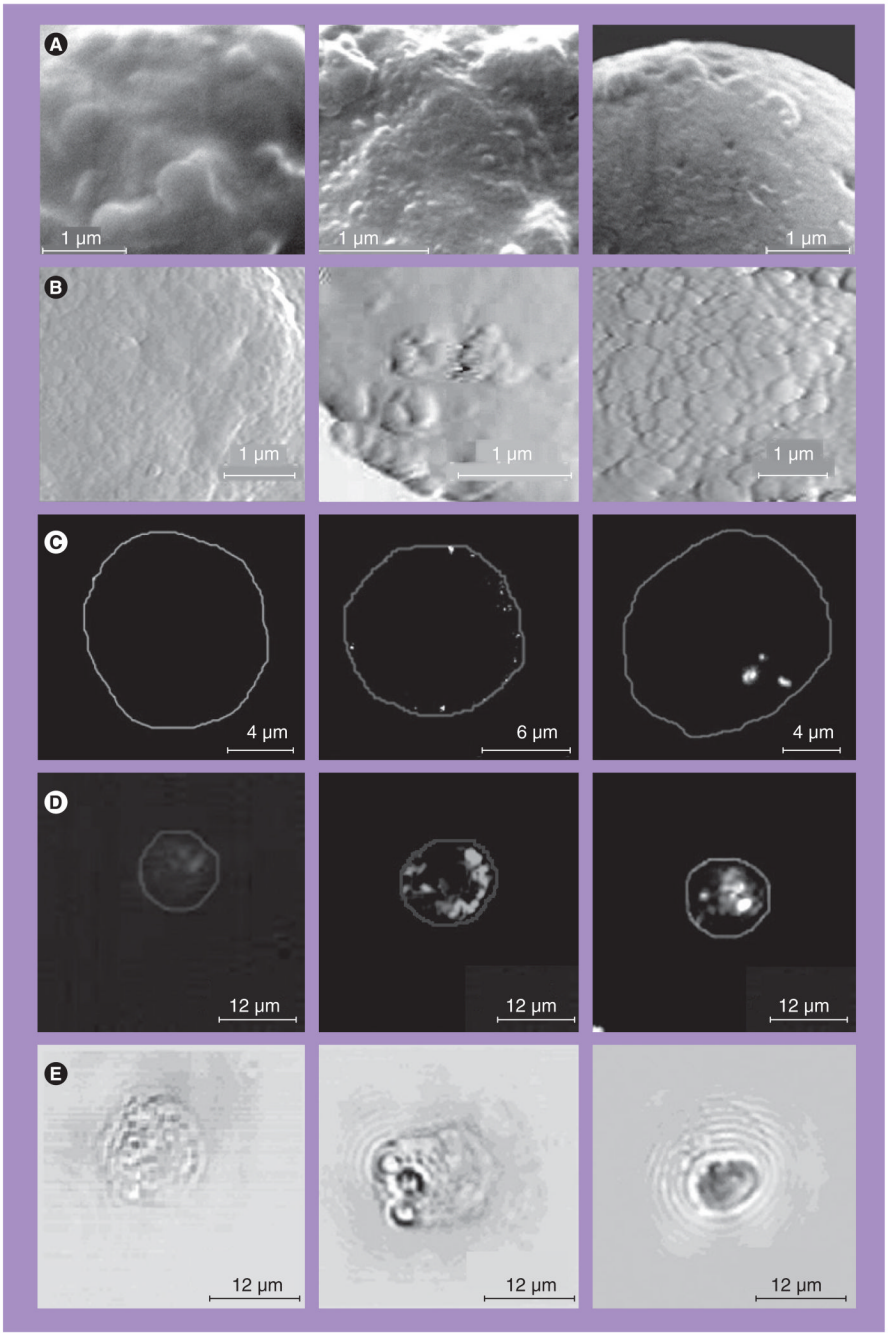

Figure 9. Images of individual K562 cells obtained before and after interaction with gold nanoparticles

Left: control; center: after targeting at 4°C with 30-nm gold nanoparticles (NPs); right: after targeting at 37°C with 30-nm gold NPs. **(A)** Images obtained with scanning electron microscope. **(B)** Images of K562 cells obtained with atomic force microscope. **(C)** Images obtained with fluorescent microscope. **(D)** Images obtained with optical side scattering microscope. **(E)** Images obtained with time-resolved photothermal microscope show the photothermal bubbles: small ones in the center image and large one in the right image, while no photothermal bubbles were detected in the left image.

Reproduced with permission from [51].

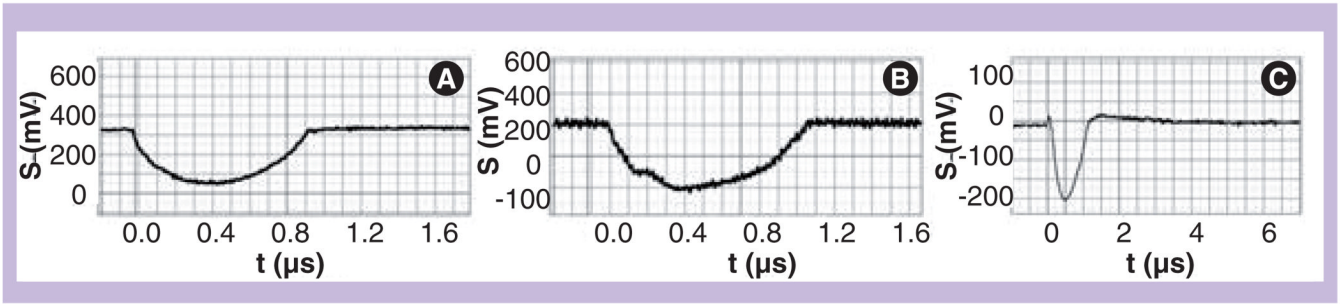

Figure 10. Time responses of the photothermal bubbles obtained with a single pump laser pulse (532 nm, 10 ns)

(A) Individual living HEP-2C cell after incubation with 70-nm gold nanorod conjugates with C225. **(B)** Individual living HEP-2C cell after incubation with 50-nm gold nanoshell conjugates with C225. **(C)** Intact lymphocyte (without any nanoparticles) and at increased fluence of pump laser pulse (27 J/cm^2).

Y-axis: signal amplitude; X-axis: Time after the pump laser pulse.

Reproduced with permission from [53].

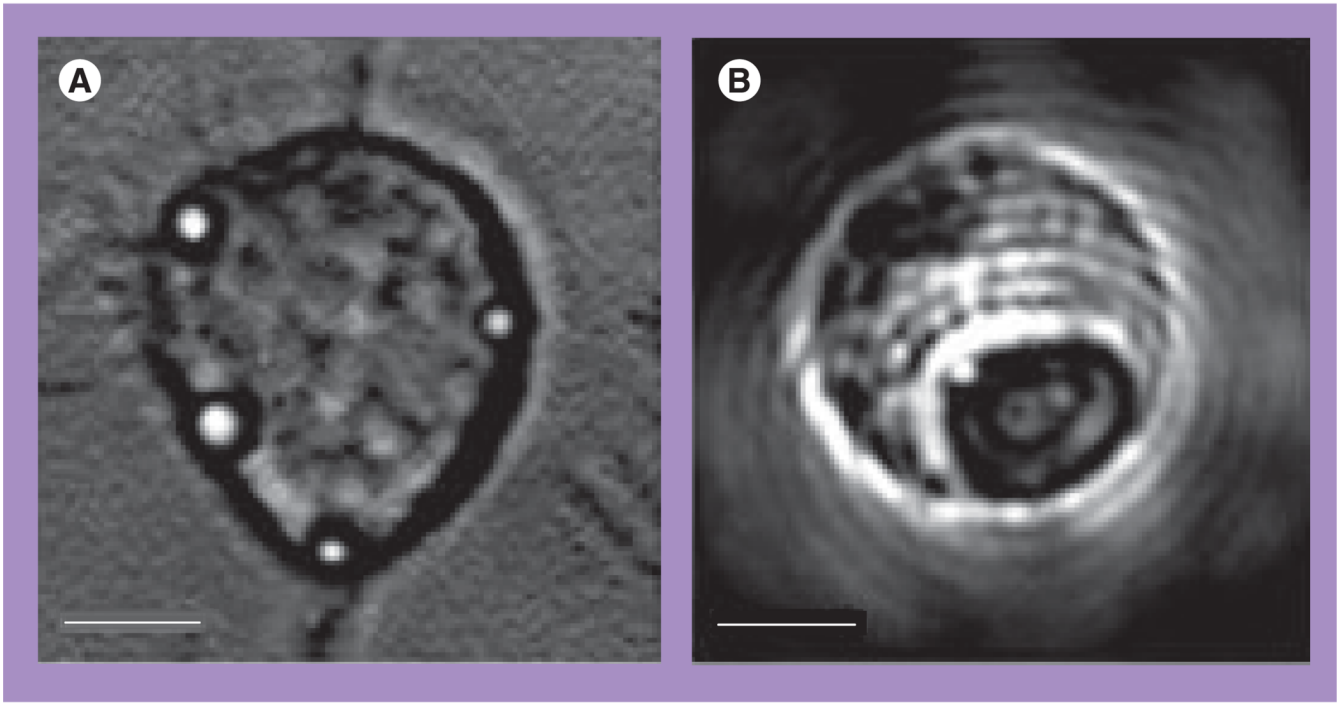

Figure 11. Nanoparticle-generated photothermal bubbles in cells

(A) A549 (C225-positive) cell with clusters of nanoshells exposed to a single laser pulse (10 ns, 750 nm, 0.7 J/cm^2). **(B)** K562 leukemia cell treated with 30-nm gold nanoparticles and a single laser pulse (10 ns, 532 nm, 1.7 J/cm^2) has yielded a big photothermal bubble. Scale bar is 10 μm.

Reproduced with permission from [53].

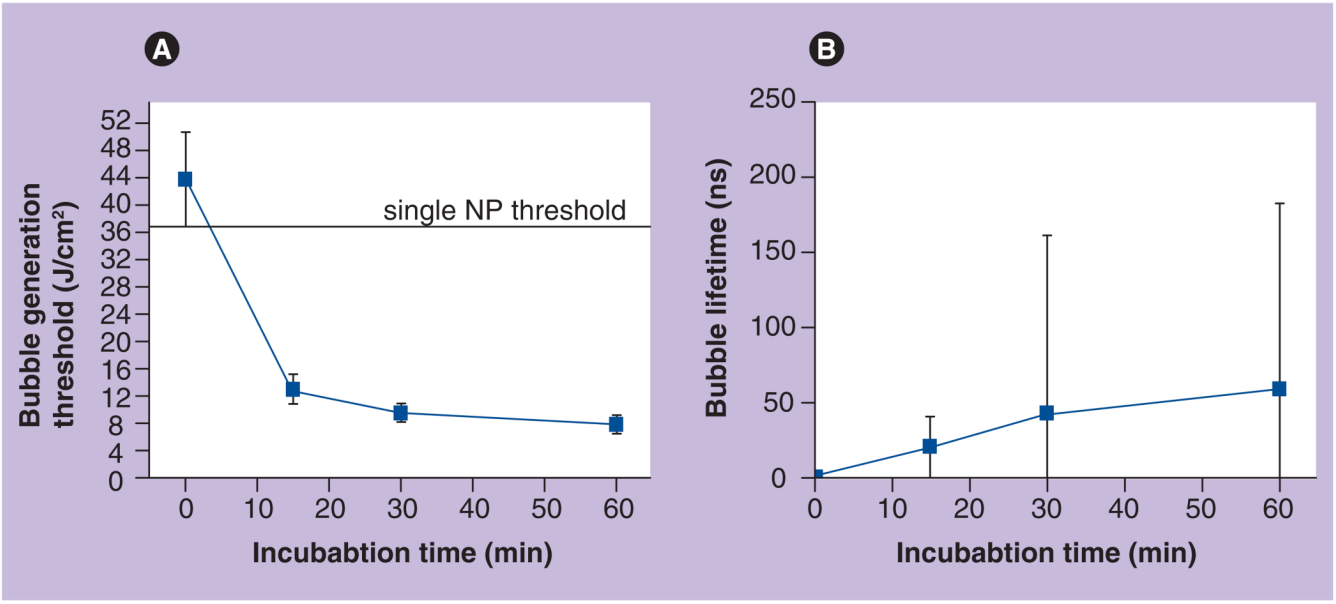

Figure 12. Time-course of two nanoparticle cluster-related parameters obtained for K562 cells with photothermal microscopy

(A) The threshold of the generation of laser-induced bubbles around clusters and **(B)** population-averaged lifetime of laser-induced bubbles around clusters (at 8 J/cm^2) as measured during incubation at 37°C with 30-nm bare gold NPs.

NP: Nanoparticle.

Reproduced with permission from [51].

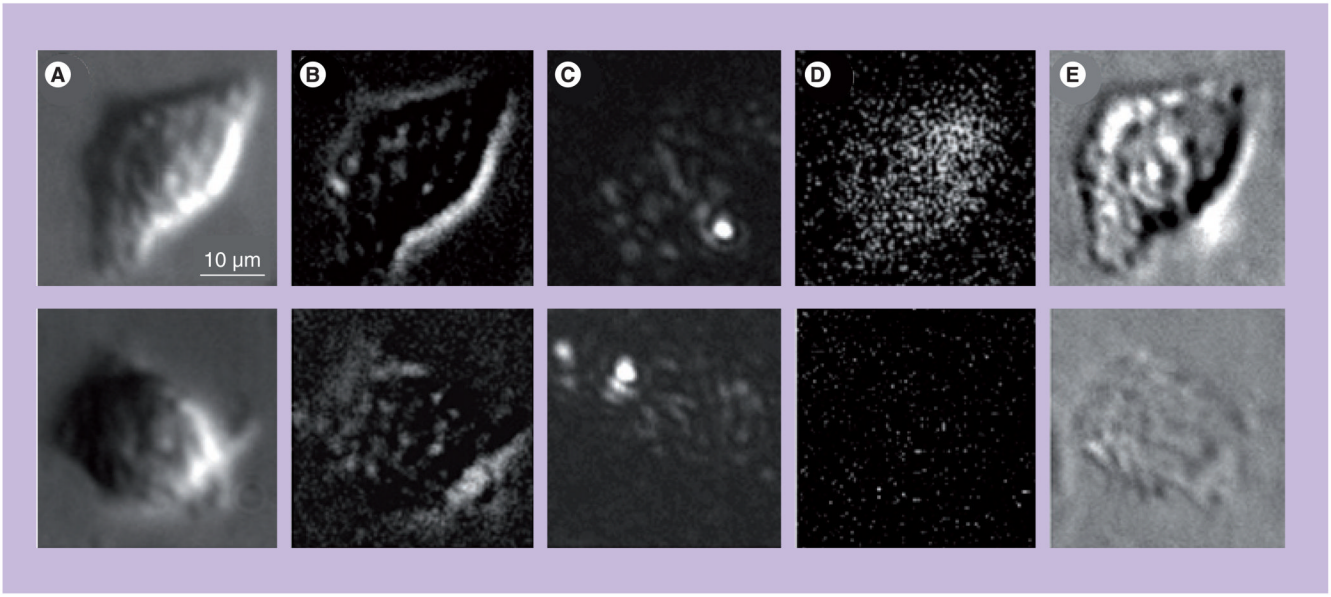

Figure 13. Images of the damaged (top panel) and surviving (bottom panel) A549 cells after their incubation with 170-nm gold nanoshells and the follow-up exposure to a single pump laser pulse that induced the photothermal bubbles

(A) White light image prior to exposure to pump laser pulse. **(B)** Side scattering image prior to exposure to pump laser pulse shows nanoshell-related signals. **(C)** Side scattering image during exposure to pump laser pulse shows photothermal bubbles. **(D)** Fluorescent image after the exposure to pump laser pulse shows epidium bromide fluorescence. **(E)** Differential white light image shows changes in the cell after exposure to pump laser pulse.
Reproduced with permission from [38].

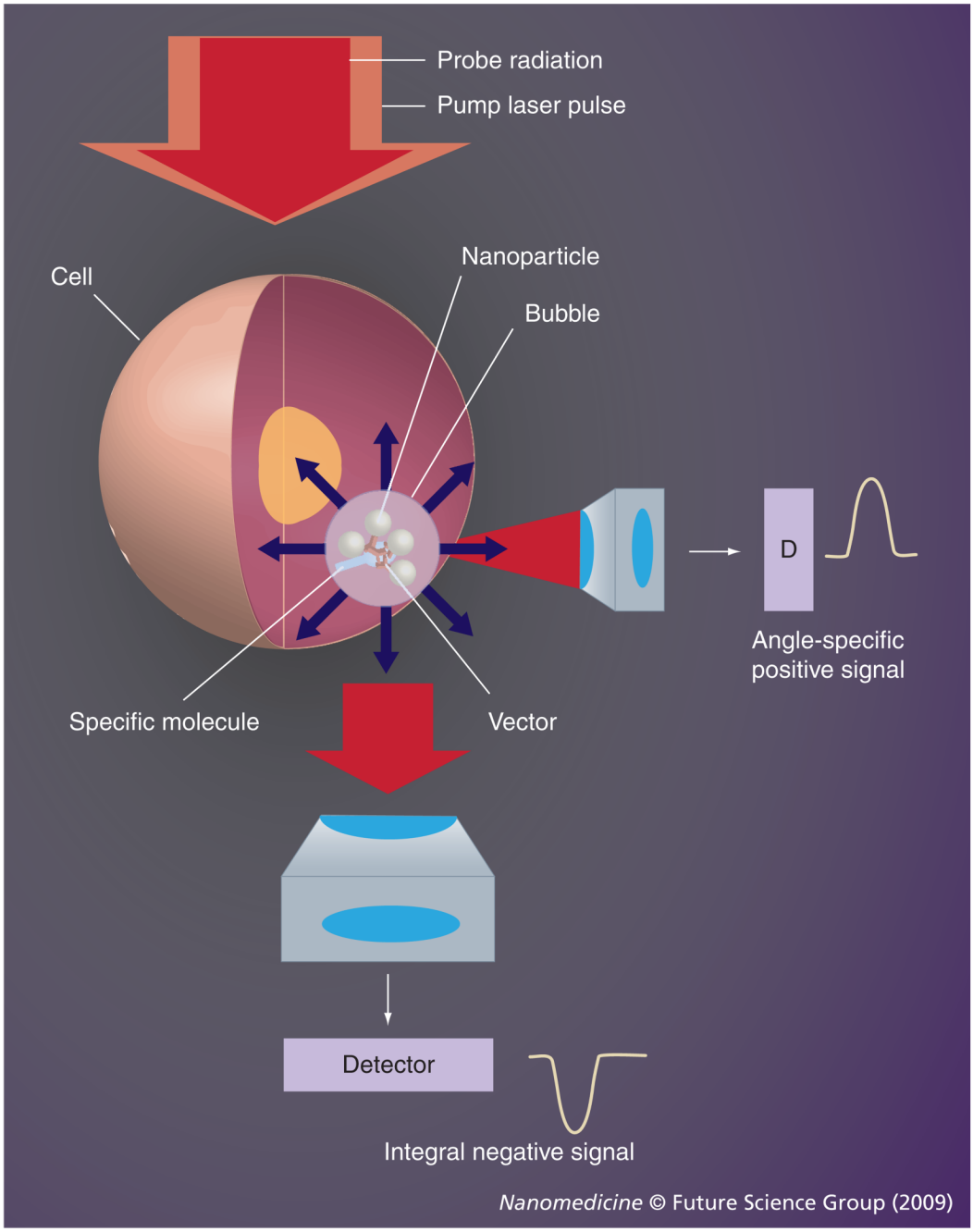

Figure 14. Principle of nanoparticle cluster–photothermal bubble mechanism of amplification of optical scattering from intracellular target

Amplitude of optical signals can be increased through formation of the target-linked nanoparticle cluster and through generation of a transient bubble around the nanoparticle cluster; photothermal bubbles may be detected with scattered probe laser beam (pulsed or continuous) as angle-specific positive signal or integral negative signal.

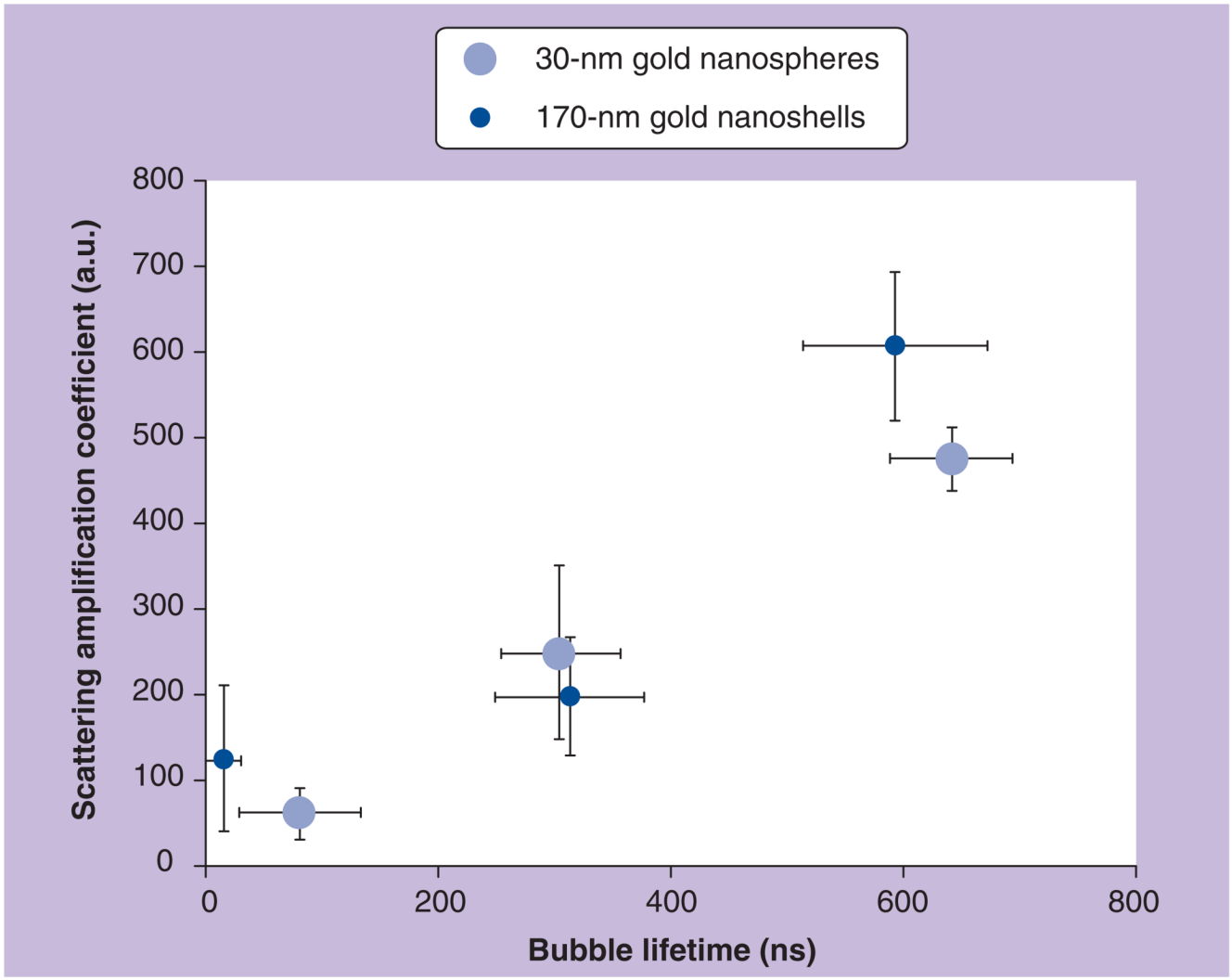

Figure 15. Dependence of optical scattering amplification coefficient upon the lifetime of the intracellular photothermal bubbles for 30-nm gold nanospheres and 170-nm gold nanoshells
Population-averaged data are given for A549 cells exposed to a single 10-ns pump pulse at 532 nm.
Reproduced with permission from [38].

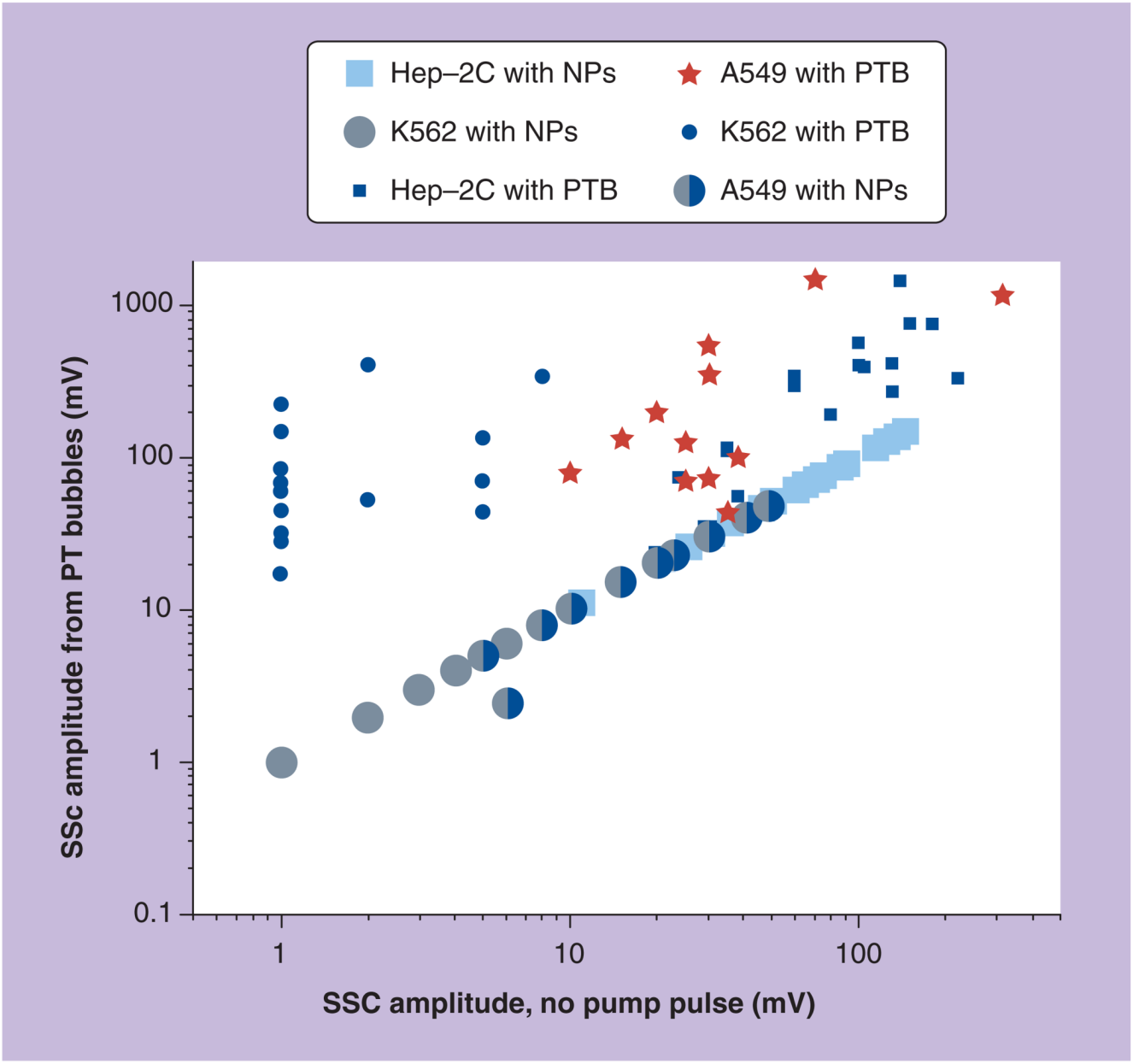

Figure 16. Diagrams of the amplitudes of integral scattering signals obtained from individual cancer cells, pretreated with 30-nm gold spherical nanoparticles, and before and during exposure to a single pump laser pulse that generates photothermal bubbles around nanoparticle clusters in the cells

NP: Nanoparticle; PTB: Photothermal bubble.

Reproduced with permission from [38].

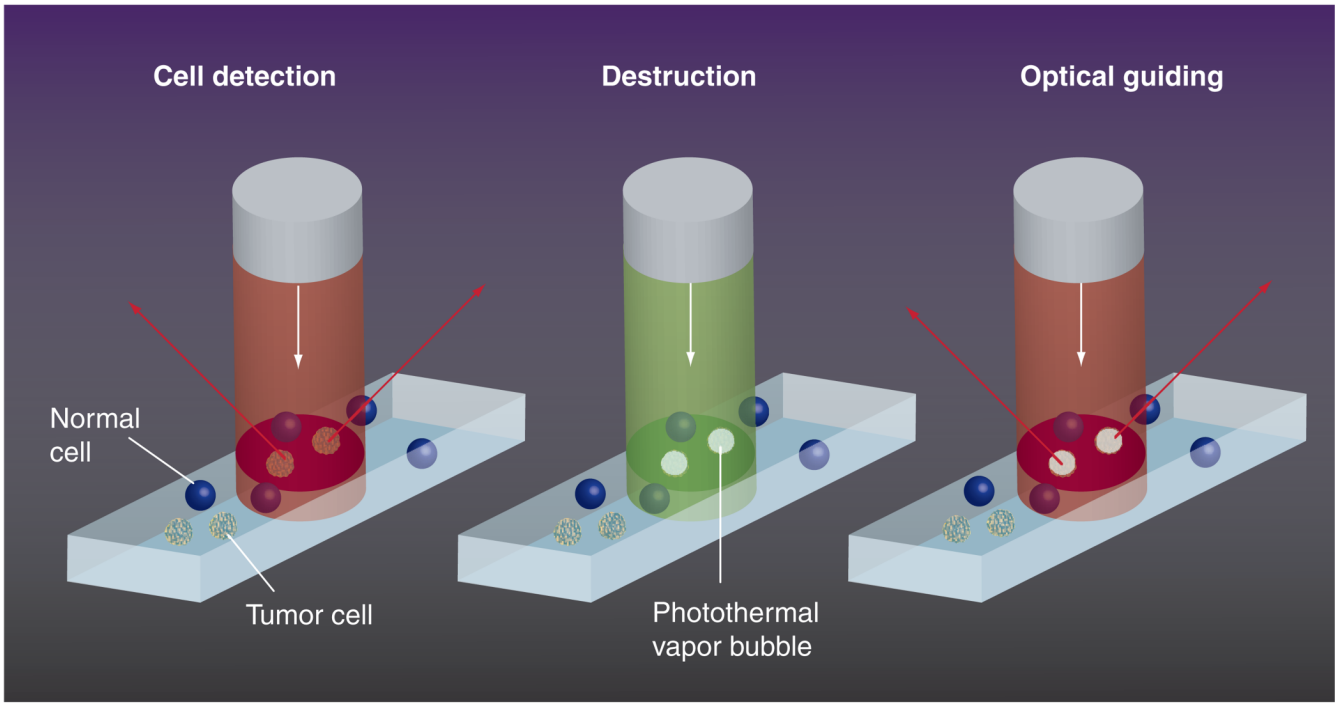

Figure 17. Laser-activated nanothermolysis as cell elimination technology (LANTCET) stages

Light-scattering detection of nanoparticle clusters in individual targeted cells with low-intensity probe laser beam (shown as red column at the left panel); damage of targeted cells with photothermal bubbles that are induced by a short laser pulse at the wavelength of nanoparticle plasmon resonance (shown as a green column at the middle panel); guidance of cell damage through optical detection of photothermal bubbles with additional probe pulse (shown as a red column at the right panel).

Reproduced with permission from [53].

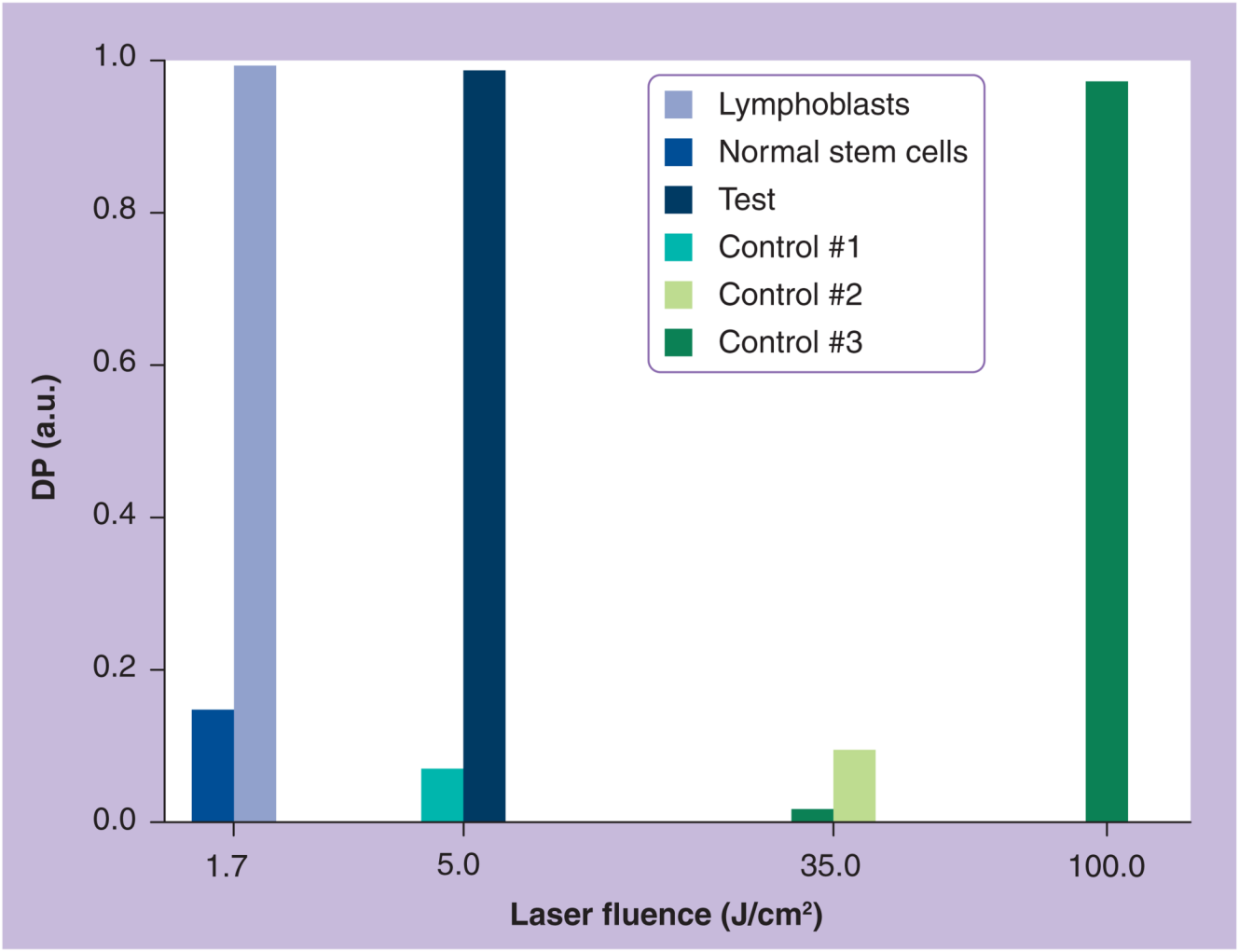

Figure 18. Cell DP experimentally obtained for different pump laser pulse (532 nm, 10 ns) fluence levels for specifically targeted common B acute lymphoblasts (lymphoblasts) and normal stem cells, for specifically targeted K562 cells (test), for nonspecifically targeted K562 cells (control 1), for K562 cells targeted with bare nanoparticle (control 2) and for untargeted K562 cells (control 3)
DP: Damage probabilities.
Reproduced with permission from [92].

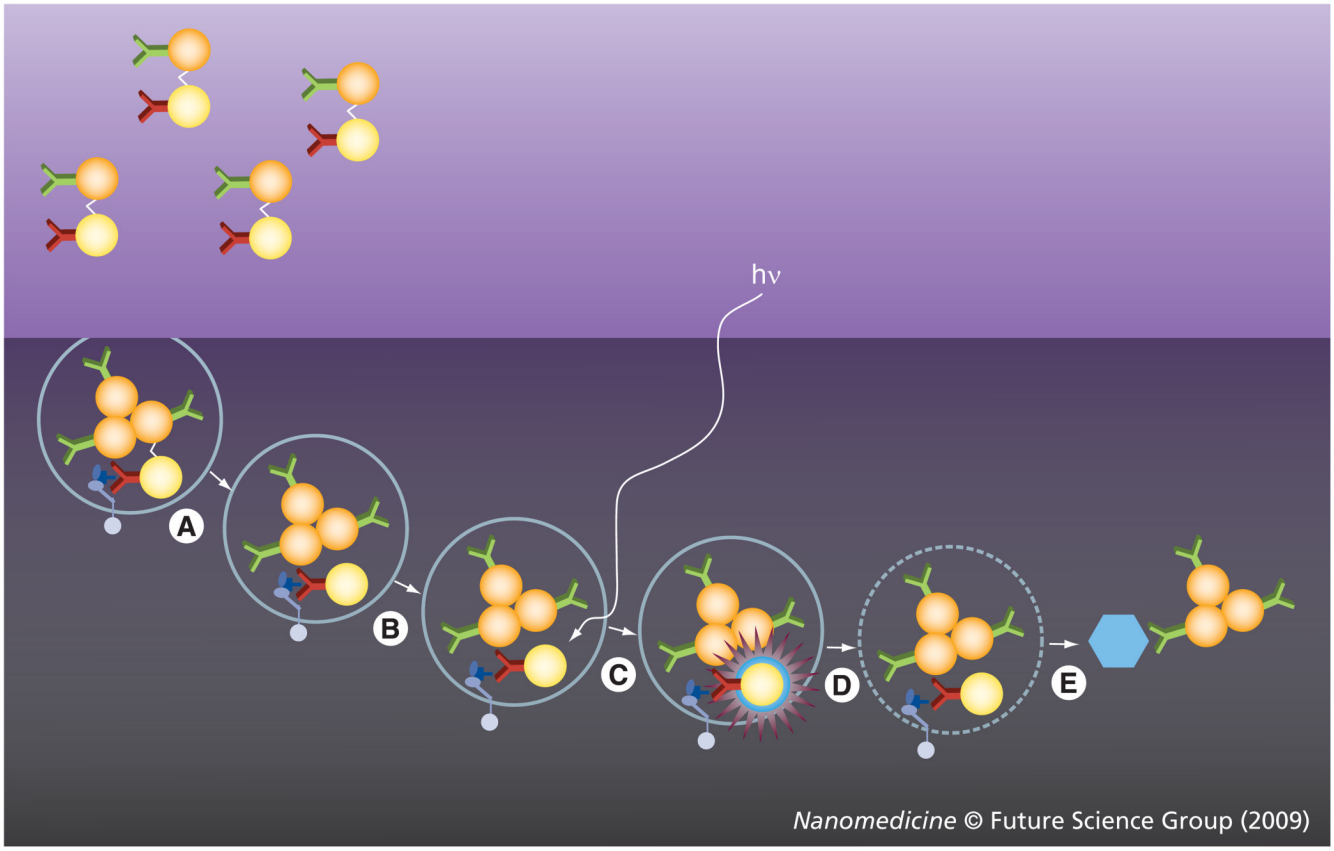

Figure 19. Photothermal bubble-based intracellular delivery

Two linked nanoparticles (NPs), NP1 (yellow) and NP2 (orange), are internalized by receptor-mediated endocytosis. For this, NP1 is conjugated to a monoclonal antibody by a target-specific vector. An antibody to a cytosolic target is attached to NP2. **(A)** Acidification of endosome cleaves the pH-sensitive links between NPs. Completion of a c vesicle forms NP clusters. **(B)** Photothermal heating NP1 clusters. **(C)** Generation of a photothermal bubble (light blue sphere). **(D)** Disruption of the endosomal membrane with subsequent release of NP2. **(E)** Association of the NP2 with a cytosolic molecular target (blue pentagon).

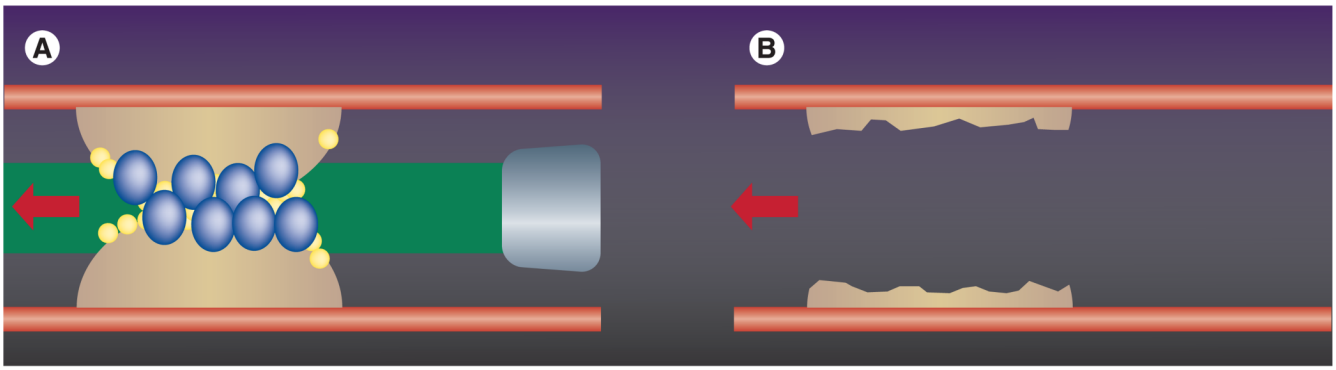

Figure 20. Principle of plaque disruption for recanalization of occluded arteries with photothermal bubbles

(A) Gold nanoparticles are injected from the catheter to the plaque site, photothermal bubbles are generated around gold nanoparticles upon irradiation with short laser pulse at the wavelength of plasmon resonance, **(B)** photothermal bubbles mechanically disrupt and remove plaque tissue, thus creating a channel in the plaque.

Reproduced with permission from [60].

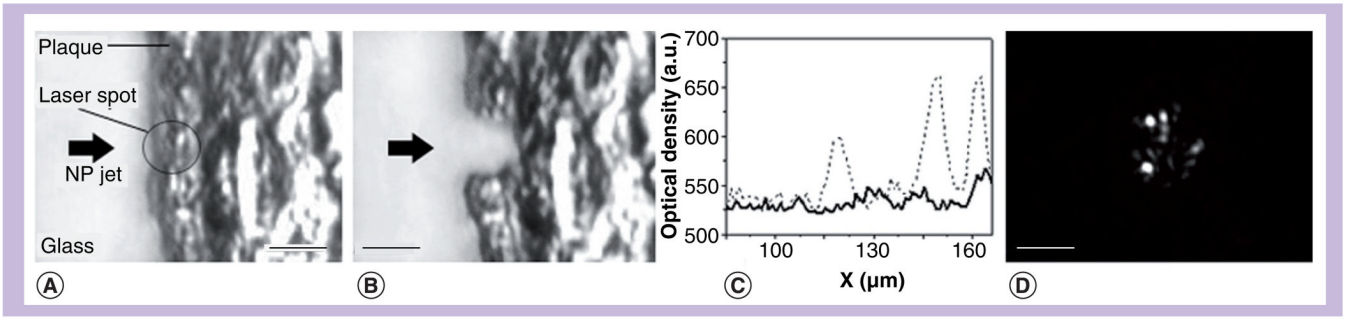

Figure 21. Elimination of the human plaque with photothermal bubbles

(A) Microscopic image of intact plaque, black arrow shows the jet of gold NPs, black circle shows the pump laser beam (532 nm, 10 ns). **(B)** Microscopic image of the same sample after exposure to laser pulses. **(C)** Optical density profiles of the intact (dashed line) and laser-treated (solid line) sample, the left part corresponds to the clear glass and the right part corresponds to the plaque tissue. **(D)** Optical side scattering images of the photothermal bubble obtained simultaneously with their generation and for the same sample. Scale bars are 20 μm.

NP: Nanoparticle.

Reproduced with permission from [60].

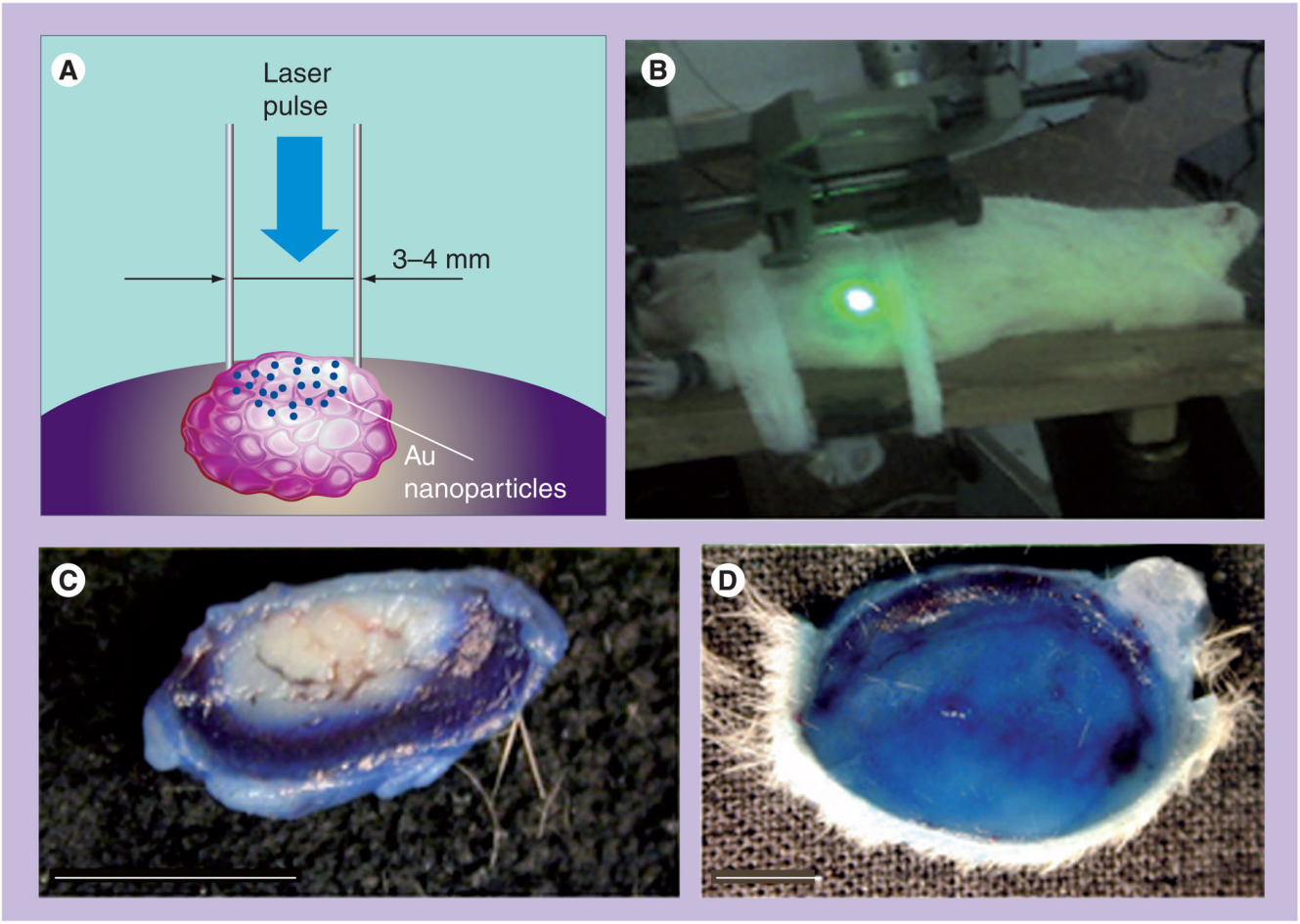

Figure 22. Scheme of the laser-activated nanothermolysis as cell elimination technology (LANTCET) treatment of the tumor in rat (A) and experimental set-up (B), vertical cross-section (slice) of the tumor: treated with nanoparticles and a single laser pulse (C), treated with laser pulse only (D)

Tumor slices were stained with Evans Blue after laser treatment and extraction from the animals (blue: intact area; white: damaged area); scale bar is 5 mm.

Reproduced with permission from [53].

Table 1

Parameters of nanoparticle-generated photothermal bubbles as measured with image and response modes for a single 0.5 ns laser pulse at 532 nm.

Optical absorber	**Single NP (30 nm)**	**Clusters of NPs (30 nm)**
I(0) (pixel counts)	546 ± 3 (within noise level)	907 ± 44
I(9ns) (pixel counts)	1134 ± 285	3998 ± 1420
S_{sc} (a.u.)	2.03 ± 0.4	12.24 ± 1.4
PTB lifetime (at 1.72 J/cm^2) (ns)	18 ± 3.5	417 ± 176
PTB threshold (J/cm^2)	0.72	0.088

I(0): Pixel image amplitude before pump pulse; I(9ns): Pixel image amplitude 9 ns after pump pulse; NP: Nanoparticle;PTB: Photothermal bubble; S_{SC}: Relative scattering amplitude at 0.9 J/cm^2.

Table 2

Nanoparticle and photothermal bubble properties for three types of gold nanoparticle.

Nanoparticles	**Gold spheres, 30 nm**		**Silica/gold shells, 170/8 nm**		**Gold rods, 45 × 14 nm**	
Excitation pulse wavelength (nm)	532 (resonance)	750 (off-resonance)	532 (off-resonance)	750 (resonance)	532 (transverse resonance)	750 (longitudinal resonance)
OD (a.u.)	1.26	0.064	0.40	1.26	0.61	2.1
PTB generation threshold fluence (J/cm^2)	5.0	60.0	0.086	0.5	7.0	20.0

OD: Optical density; PTB: Photothermal bubble.

Table 3

Comparison of the process of generation of the photothermal bubbles around plasmonic nanoparticles and in homogeneously absorbing media.

Experimental parameters	Laser pulse duration	Environmental bulk heating	Size of the absorber
Plasmonic NP in transparent suspension	++	−	PTB threshold fluence decreases
Homogenous and micrometer-size optical absorbers	+	+	PTB threshold fluence increases

+: Indicates influence of specific experimental parameter.
NP: Nanoparticle; PTB: Photothermal bubble.

Table 4

Parameters of $CD33^{+}$ leukemia cells that have been targeted with 30-nm gold nanoparticles.

Method	Fluorescent Flow cytometry	Fluorescent microscopy	Atomic force microscopy	Light scattering microscopy	Scanning electron microscopy
Size-sensitive parameter	Fluorescent intensity (counts)	Pixel image amplitude (counts)	NP cluster size (nm)	Pixel image amplitude (counts)	NP cluster size (nm)
Intact cells	63 ± 46	110 ± 47	0	620 ± 110	0
NP-treated cells, membrane targeting at 4°C	164 ± 78	564 ± 127	300–600	3450 ± 1650	100–400
NP-treated cells, targeting at 37°C	121 ± 83	832 ± 592	n/a	9200 ± 4770	100–600

NP: Nanoparticle.

Nanomedicine (Lond). Author manuscript; available in PMC 2010 August 1.

Table 5

Photothermal bubble generation threshold fluences for single 10-ns laser pulse.

Cell	K562 (leukemia)	Human bone marrow myeloblasts (leukemia)	Human bone marrow myeloblasts (leukemia)	Hep2C, A549 (squamous carcinoma)	Lymphocytes (blood cell)
NP	Gold spheres 30 nm at 532 nm	Gold spheres 30 nm at 532 nm	Gold rods 14 × 45 nm at 750 nm	Silica-gold shells 50 nm at 750 nm	Silica-gold shells 50 nm at 750 nm
Single NPs (in water)	14.0	14.0	12	11.0	11.0
Nonspecifically targeted cells (bare NPs)	5.0	2.1	1.5	11.0	
Specifically targeted cells (antibody conjugated to NPs) via receptor-mediated endocytosis	0.3 (CD33)	0.3 (CD33)	0.32 (PEG)	0.5 (C225)	12.0 ± 1.2
Intact cells	50–70	35–50	35–50	>40	>40

NP: Nanoparticle.

Table 6

Lifetimes (ns) of photothermal bubbles generated with single laser pulse around nanoparticles and nanoparticle clusters in water suspensions and in individual tumor cells.

NP	Laser pulse		Suspension of single NPs	Suspension of NP clusters	Cells	
	Fluence (J/cm^2)	Wavelength (nm)		Hep-2C	Hep-2C	A549
NSP: spheres 39.5 nm	1.3	532	10 ± 4	356 ± 173	460 ± 542	480 ± 557
NR: rods 13.6 × 45.9 nm	0.56	750	0	190 ± 152	–	115 ± 130
NS: shells 171 nm	0.56	750	25 ± 20	470 ± 184	–	104 ± 46

NP: Nanoparticle; NR: Nanorod; NS: Nanoshell; NSP: Nanosphere.

Table 7

Comparison of the features of two optical scattering methods for sensing photothermal bubbles.

Detection method	Pros	Cons
Time-resolved image mode	High sensitivity	Requires precise focusing due to small size of PTB
	Shows 2D location of the PTB	Saturates when PTB size reaches some threshold
	Pixel image amplitude is PTB size-dependent	
	Pixel image amplitude can be amplified by increasing	
	pulse fluence	
Response mode	Allows detection of the PTB in 3D volume regardless	Relatively low sensitivity
	of its specific position	Signal duration slightly depends upon the number
	Signal duration is PTB size-dependent	of the PTBs in the aperture of the probe beam
	Does not saturate when PTB size reaches	
	some threshold	
	Allows detection of other PT phenomena such as	
	heating of the bulk media	

PT: Photothermal; PTB: Photothermal bubble.